This is the preprint of the following article:
M. Gameiro, J.P. Lessard, A. Pugliese
Computation of smooth manifolds via rigorous multi-parameter continuation in infinite dimensions
Found. Comput. Math., Volume 16, Issue 2, pp 531-575, 2016
DOI: https://doi.org/10.1007/s10208-015-9259-7

Computation of smooth manifolds via rigorous multi-parameter continuation in infinite dimensions

Marcio Gameiro* Jean-Philippe Lessard† Alessandro Pugliese ‡

Abstract

In this paper, we introduce a constructive rigorous numerical method to compute smooth manifolds implicitly defined by infinite dimensional nonlinear operators. We compute a simplicial triangulation of the manifold using a multi-parameter continuation method on a finite dimensional projection. The triangulation is then used to construct local charts and an atlas of the manifold in the infinite dimensional domain of the operator. The idea behind the construction of the smooth charts is to use the radii polynomial approach to verify the hypotheses of the uniform contraction principle over a simplex. The construction of the manifold is globalized by proving smoothness along the edge of adjacent simplices. We apply the method to compute portions of a two-dimensional manifold of equilibria of the Cahn-Hilliard equation.

1 Introduction

Partial differential equations (PDEs), delay differential equations (DDEs) and ordinary differential equations arising from physics, biology, chemistry, economics or engineering often depend on parameters. It is, therefore, natural to study the changes in the qualitative behavior of the solutions as one changes some parameters in the equations. Thus, it is not surprising that there is a vast literature on numerical techniques devoted to continuation of such solutions, often in the form of predictor-corrector algorithms. In the context of infinite dimensional problems like PDEs and DDEs, the continuation algorithms have to be performed on a finite dimensional projection, which raises the natural question of the validity of the outputs. In order to address this fundamental question, rigorous one-parameter continuation methods have been proposed to compute global branches of solutions of PDEs and DDEs [1, 2, 3, 4, 5]. While these methods have been applied to compute one-dimensional manifolds, we are not aware of any rigorous method aiming at computing solution manifolds of dimension greater than one. In this regard, we propose here a rigorous multi-parameter continuation method to compute smooth two-dimensional manifolds implicitly defined by zeros of nonlinear operators defined on infinite dimensional Banach spaces. More explicitly, we are interested in the following general problem.

*Instituto de Ciências Matemáticas e de Computação, Universidade de São Paulo, Caixa Postal 668, 13560-970, São Carlos, SP, Brazil (e-mail address: gameiro@icmc.usp.br). This author was partially supported by FAPESP, CAPES and CNPq, Brazil.

†Université Laval, Département de Mathématiques et de Statistique, 1045 avenue de la Médecine, Québec, QC, G1V 0A6, CANADA (jean-philippe.lessard@mat.ulaval.ca).

‡Dipartimento di Matematica, Università degli Studi di Bari Aldo Moro, Via E. Orabona 4, 70125 Bari, ITALY (alessandro.pugliese@uniba.it). This author was supported in part by INdAM – GNCS.

Problem Definition: *Let B_1, B_2 two Banach spaces (possibly infinite dimensional), and a nonlinear operator $f : \mathbb{R}^2 \times B_1 \to B_2$ which is assumed to be compact and twice Fréchet differentiable. Let $\mathcal{M} \subset \mathbb{R}^2 \times B_1$ a set that satisfies the two assumptions*

- $\mathcal{M} \subset \big\{x \in \mathbb{R}^2 \times B_1 : f(x) = 0\big\}$,
- $\forall\ x \in \mathcal{M}$, *the linear operator $Df(x) : \mathbb{R}^2 \times B_1 \to B_2$ has a bounded inverse.*

The general goal of this paper is to introduce a method to rigorously compute local charts and an atlas for the two-dimensional manifold $\mathcal{M}$.

Our main motivation for developing such method comes from the study of finite and infinite dimensional parameter dependent dynamical systems. From the point of view of dynamical systems, the objects of interest are bounded solutions that exist globally in time, for instance, equilibria (steady states), time periodic solutions, solutions of boundary value problems, connecting orbits, etc. For a large class of problems, these solutions are more regular than the typical solutions of the phase space. Based on this a priori knowledge of regularity, spectral methods can be used to define a nonlinear operator $f : \mathbb{R}^2 \times B_1 \to B_2$ such that a solution $x = (p, a) \in \mathbb{R}^2 \times B_1$ of

$$f(x) = 0 \tag{1}$$

corresponds to a bounded solution of interest. The domain of f contains the parameter space $\mathbb{R}^2$ and B_1, B_2 are infinite dimensional Banach spaces of fast decaying coefficients (modes). In case the targeted solution has a periodic profile, the infinite dimensional vector $a = (a_k)_k$ may be the coefficients of the Fourier expansion of the solution, while, if the solution has a non periodic profile, the infinite dimensional vector a may be the coefficients of the Chebyshev polynomials expansion of the solution.

An overview of the individual steps that need to be performed to rigorously compute local charts and an atlas for the manifold $\mathcal{M}$ is the following.

1. The problem (1) is reduced to a finite dimensional one using a spectral Galerkin projection. See (5) for the details of this finite dimensional projection.

2. A simplex-based multi-parameter continuation technique is performed on the finite dimensional projection to obtain an approximate simplicial triangulation $\mathcal{S}$ of the manifold. The algorithm is presented in Section 3.

3. For each simplex $\sigma \in \mathcal{S}$, the existence of a genuine smooth local chart U_σ of the solution manifold in the original infinite dimensional space is obtained. The local chart U_σ is guaranteed to exist with precise and explicit bounds in the Banach space around σ. In practice, this crucial step is done by constructing the radii polynomials as defined in Definition 2.4 and by applying Lemma 2.5. The radii polynomial approach provides an efficient way of verifying that a certain Newton type operator is a uniform contraction on a *thin* set centered at a simplex. The construction of the polynomials is presented in Section 2.2, and requires developing analytic estimates that control the truncation error terms (the tail part) involved in computing the approximate simplices using a finite dimensional projection. The analytic estimates are presented in Appendix A.

4. We demonstrate that for each $\sigma \in \mathcal{S}$, the chart U_σ is smooth. This is done by verifying the hypothesis (31) of Lemma 2.6 of Section 2.3 with interval arithmetic.

5. The final step is to demonstrate that the set of smooth local charts $\{U_\sigma\}_{\sigma\in\mathcal{S}}$ forms a global smooth atlas. This is obtained from the conclusion of Theorem 4.2. This step is theoretical and does not require any computation. As one can see in the proof of Theorem 4.2, the conclusion follows from the previous steps. Combining all the above, we have a constructive proof that the set

$$\mathcal{M} \stackrel{\text{def}}{=} \bigcup_{\sigma\in\mathcal{S}} U_\sigma$$

is a smooth two-dimensional manifold embedded in the Banach space $\mathbb{R}^2 \times B_1$.

Let us mention that multi-parameter continuation algorithms have already been proposed to compute numerical approximations for smooth manifolds implicitly defined by finite dimensional nonlinear equations [6, 7, 8, 9, 10]. In fact, the simplex-based multi-parameter continuation algorithm that we propose to compute the manifold is strongly inspired by the work of [7, 8]. Although we follow the main philosophy of the algorithm in [7, 8], we introduce several novelties that improve its robustness and make it suitable for our purposes. The main distinguishing features of our algorithm are described in Remark 3.1. The verification method based on the uniform contraction principle on each simplex is inspired by the pseudo-arclength continuation methods introduced in [1, 11] for smooth one-dimensional manifolds.

Remark 1.1. The reason why we opted for Brodzik and Rheinboldt's continuation approach will be illustrated at the beginning of Section 3. However, we point out that, in principle, different continuation schemes could also be adapted to fit the needs of our method.

Remark 1.2. The main idea behind our method is not specific to spectral Galerkin projections. In fact, the conditions that allow the rigorous continuation of the solution manifold (i.e. the "Y and Z bounds" (11) and (12) that appear in Lemma 2.2) are akin to the hypothesis of the Newton-Kantorovich Theorem: uniform bounds on, respectively, the inverse and the second derivative of a certain operator. These, in turn, are reminiscent of the "stability and consistency" conditions of the Lax Equivalence Theorem. We decided to present our method in the context of spectral Galerkin discretizations because the explicit analytic estimates required to control the truncation error terms (the tail part) involved in computing on a Galerkin projection have been recently developed within the field of rigorous numerics (e.g. see [11, 13]).

The paper is organized as follows. In Section 2, we present the rigorous method to compute local smooth charts of two-dimensional manifolds implicitly defined by a C^ℓ operator f, with $\ell \geq 2$. In Section 3, we introduce the algorithm to construct the finite dimensional simplicial approximation of the manifold. We show in Section 4 how to combine the methods of Section 2 and Section 3 to *glue* the charts and therefore construct rigorously the atlas of the smooth manifold. In Section 5, we apply the method to rigorously compute a two-dimensional manifold of equilibria of the Cahn-Hilliard PDE defined on a one-dimensional spatial domain with Neumann boundary conditions. In Section 6, we conclude and present some potential future applications, as well as extensions to the present work.

The Appendix A provides the necessary convolution estimates required to construct the radii polynomials for the Cahn-Hilliard equation studied in Section 5. We decided to include all formulas and proofs so that the paper is self-contained. Note, however, that these analytic convolution estimates are taken directly from [15].

2 Rigorous computation of the local charts

In this section, we develop a systematic rigorous computer-assisted approach to construct local charts for two-dimensional manifolds $\mathcal{M} \subset \left\{x \in \mathbb{R}^2 \times B_1 : f(x) = 0\right\}$. More precisely, we introduce an algorithm that provides precise bounds in the Banach space $\mathbb{R}^2 \times B_1$ around an approximate simplex within which a genuine smooth local chart of the manifold is rigorously guaranteed to exist. The bounds are obtained with the use of the radii polynomial approach, which provides an efficient means of determining a domain on which the uniform contraction mapping theorem is applicable. The next section presents this approach.

2.1 The radii polynomial approach

In order to define the radii polynomials, we need to define explicitly the Banach spaces B_1 and B_2 on which the proofs of existence of the charts are going to be obtained. Recall that a solution $x = (p, a)$ of $f(x) = 0$ is composed of a parameter $p \in \mathbb{R}^2$ and an infinite dimensional vector $a = (a_k)_{k\geq 0}$ of coefficients of the (Fourier or Chebyshev) expansion of the a priori unknown solution of interest. As already mentioned in Section 1, due to the regularity of the solutions, the decay rate of the coefficients is fast. In fact, if the targeted solution is analytic, the decay rate of its coefficients is faster than any algebraic decay. Considering weights ω_k^q with algebraic growth rate q defined by

$$\omega_k^q \stackrel{\text{def}}{=} \begin{cases} 1, & \text{if } k = -2, -1, 0 \\ k^q, & \text{if } k > 0, \end{cases} \tag{2}$$

define the norm

$$\|a\|_q \stackrel{\text{def}}{=} \sup_{k\geq 0} \left\{|a_k|\omega_k^q\right\}, \tag{3}$$

which is then used to define the Banach space

$$\Omega^q = \{a = (a_k)_{k\geq 0} : \|a\|_q < \infty\}. \tag{4}$$

Define the spaces $B_1 = \Omega^q$ and $B_2 = \Omega^{q'}$ for some decay rates $q, q' \in \mathbb{R}$, and let

$$X \stackrel{\text{def}}{=} \mathbb{R}^2 \times \Omega^q.$$

Given $x \in X$, denote $x_{-2} = p_1$, $x_{-1} = p_2$ and $x_k = a_k$, for $k \geq 0$. For $x = (p, a) = (p_1, p_2, a) \in X$, define a norm on X by

$$\|x\|_X = \sup_{k\geq -2} \left\{|x_k|\omega_k^q\right\} = \max\{|p_1|, |p_2|, \|a\|_q\}.$$

Using this construction, $(X, \|\cdot\|_X)$ is a Banach space. Assume that $f\colon X \to \Omega^{q'}$ is a C^ℓ function. In order to construct local charts of a two-dimensional manifold $\mathcal{M} \subset \{x \in X : f(x) = 0\}$, we consider first a finite dimensional reduction of f that we denote by

$$f^{(m)} : \mathbb{R}^{m+2} \to \mathbb{R}^m. \tag{5}$$

Essentially, $f^{(m)}$ consists of keeping the first $m + 2$ coordinates of x and the first m components of f. Assume that, using a Newton-like iterative method, we computed three points $\bar{x}_0, \bar{x}_1, \bar{x}_2 \in \mathbb{R}^{m+2}$ approximately on $\mathcal{M}$, that is, $f^{(m)}(\bar{x}_i) \approx 0$ $(i = 0, 1, 2)$. Assume also that $Df^{(m)}(\bar{x}_i) \in \mathcal{L}(\mathbb{R}^{m+2}, \mathbb{R}^m)$ has a two dimensional kernel, or, equivalently,

that it has full rank. Hence, for each $i = 0, 1, 2$, assume the existence of linearly independent $\phi_1^i, \phi_2^i \in \mathbb{R}^{m+2}$ such that $Df^{(m)}(\bar{x}_i)\phi_j^i = 0$ for $j = 1, 2$. For each $i = 0, 1, 2$, define $\bar{\Phi}_i = [\phi_1^i \ \phi_2^i] \in \mathbb{R}^{m+2} \times \mathbb{R}^{m+2}$. Note that, in practice, for $i = 0, 1, 2$, the ϕ_j^i's will be computed such that they are mutually orthonormal vectors (we refer to Section 3.1.3 for details about how they are computed). As a consequence of the above construction, the plane spanned by ϕ_1^i and ϕ_2^i is the tangent plane $\mathcal{T}_{\bar{x}_i}\mathcal{M}$ to the surface $\mathcal{M}$ at the point $\bar{x}_i$ $(i = 0, 1, 2)$ and

$$\begin{pmatrix} Df(\bar{x}_i) \\ \bar{\Phi}_i^T \end{pmatrix} \bar{\Phi}_i = \begin{pmatrix} 0 \\ I \end{pmatrix}.$$

Now, let

$$\Delta \stackrel{\text{def}}{=} \{s = (s_1, s_2) \mid s_1, s_2 \geq 0 \text{ and } s_1 + s_2 \leq 1\}.$$

Assuming that $\bar{x}_1 - \bar{x}_0$ and $\bar{x}_2 - \bar{x}_0$ are linearly independent, the following is a one-to-one parameterization of a 2-dimensional simplex σ with vertices $\bar{x}_0$, $\bar{x}_1$ and $\bar{x}_2$:

$$\bar{x}_s \stackrel{\text{def}}{=} \bar{x}_0 + s_1(\bar{x}_1 - \bar{x}_0) + s_2(\bar{x}_2 - \bar{x}_0), \quad s = (s_1, s_2) \in \Delta. \tag{6}$$

Formally, the simplex is defined as

$$\sigma \stackrel{\text{def}}{=} \bigcup_{s \in \Delta} \{\bar{x}_s\}.$$

For $\bar{x}_s \in \mathbb{R}^{m+2}$, we identify $(\bar{x}_s, 0_\infty) \in X$ with $\bar{x}_s$, where 0_∞ is the infinite dimensional vector with coordinates all equal to zero. Consider the interpolation of the two-dimensional kernels $\bar{\Phi}_0$, $\bar{\Phi}_1$ and $\bar{\Phi}_2$ defined by

$$\bar{\Phi}_s \stackrel{\text{def}}{=} \bar{\Phi}_0 + s_1(\bar{\Phi}_1 - \bar{\Phi}_0) + s_2(\bar{\Phi}_2 - \bar{\Phi}_0), \quad s = (s_1, s_2) \in \Delta. \tag{7}$$

As above, depending on the context, $\bar{\Phi}_s \in \mathbb{R}^{m+2} \times \mathbb{R}^{m+2}$ or $\bar{\Phi}_s \in X \times X$. Consider now $\bar{\Phi}_s^T \in \mathcal{L}(X, \mathbb{R}^2)$ as a linear transformation between X and $\mathbb{R}^2$. Define the Banach space $W = \mathbb{R}^2 \times \Omega^{q'}$ and define $\mathcal{F}_s : X \to W$ by

$$\mathcal{F}_s(x) = \begin{pmatrix} \bar{\Phi}_s^T(x - \bar{x}_s) \\ f(x) \end{pmatrix}. \tag{8}$$

Note that, for a given $s \in \Delta$, a solution x of $\mathcal{F}_s(x) = 0$, if it exists, is the projection of $\bar{x}_s \in \sigma$ onto $\mathcal{M}$ orthogonally to σ. Our goal is now to find zeros of (8). Rather than working with (8) directly, we recast the problem as a fixed point problem, essentially given by a Newton-like operator defined on the full Banach space X. In order to obtain such operator, we introduce an approximate inverse for $\Delta\mathcal{F}_s$ at an approximate solution. Define

$$\mathcal{F}_s^{(m)}(x) = \begin{pmatrix} \bar{\Phi}_s^T(x - \bar{x}_s) \\ f^{(m)}(x) \end{pmatrix}.$$

Essentially, $\mathcal{F}^{(m)} : \mathbb{R}^{m+2} \to \mathbb{R}^{m+2}$ consists of keeping the first $m + 2$ coordinates of x and the first $m + 2$ components of $\mathcal{F}$.

Assume that, with the help of the computer, we have computed explicitly

$$A_m \approx \left(D\mathcal{F}_0^{(m)}(\bar{x}_0)\right)^{-1},$$

a numerical inverse of $D\mathcal{F}_0^{(m)}(\bar{x}_0)$. Furthermore, assume that we have verified that A_m is invertible (this hypothesis can be rigorously verified through the use of interval arithmetic).

Given $x \in X$, denote $x_F = (x_{-2}, x_{-1}, \ldots, x_{m-1})$. Finally, define the linear operator $A : W \to X$ by

$$(Ax)_k = \begin{cases} (A_m x_F)_k, & k = -2, \ldots, m-1 \\ \mu_k^{-1} x_k, & k \geq m, \end{cases} \tag{9}$$

where $\mu_k \stackrel{\text{def}}{=} \frac{\partial f_k}{\partial x_k}(0)$. We make the assumption that $|\mu_k| \to \infty$ as $k \to \infty$. Note, for instance, that this assumption is verified when the operator (1) is obtained by expanding in Fourier series the solutions of a semi-linear parabolic PDE defined on an interval. More explicitly, given the equation

$$\partial_t u = Lu + N(u, \partial_y u, \ldots, \partial_y^{n-1} u),$$

where L is a linear differential operator of order n in the spatial variable y and N is a polynomial, the linear part μ_k in Fourier space corresponding to L dominates the nonlinear part, and grows faster to infinity. We refer to Section 5 and to (42) for an explicit example in the context of the fourth order Cahn-Hilliard equation. Assuming that m is taken large enough so that $|\mu_k| > 0$ for all $k \geq m$, one gets that A defined by (9) is an invertible linear transformation.

Remark 2.1. The assumption that $|\mu_k| > 0$ for all $k \geq m$ may seem unecessary since $|\mu_k| \to \infty$ as $k \to \infty$. However, for a given parameter dependent problem, it is possible that the linear part $\mu_k = \mu_k(\lambda)$ depends on a parameter λ, and that for every k, there exists λ_k such that $\mu_k(\lambda_k) = 0$, with $\lambda_k \to \infty$ as $k \to \infty$. That is the case for instance for the Cahn-Hilliard equation considered in Section 5, where $\mu_k(\lambda) = 1 - \pi^2 k^2/\lambda$. In this case, $\lambda_k = \pi^2 k^2$. Hence, for a fixed parameter value λ, we have to choose m large enough so that $\mu_k(\lambda) \neq 0$, for all $k \geq m$.

The idea behind the choice of operator (9) is that for large enough projection dimension m, one should have that $A \approx D\mathcal{F}_0(\bar{x}_0)^{-1}$. Indeed, since we know a priori that the coefficients of the (Fourier or Chebyshev) expansion of the bounded solutions of interest decay fast, the off-diagonal terms in $D\mathcal{F}_0(\bar{x}_0)$ of the form $\frac{\partial f_k}{\partial x_l}$ should rapidly go to zero as $|k-l|$ grows. Since $|\mu_k| \to \infty$ as $k \to \infty$, the operator $D\mathcal{F}_0(\bar{x}_0)$ should be asymptotically diagonally dominant. Hence, at least in principle, the larger m is, the better A is as an approximation of $D\mathcal{F}_0(\bar{x}_0)^{-1}$. Using the approximate inverse A given by (9), define $T_s : X \to X$ by

$$T_s(x) = x - A\mathcal{F}_s(x). \tag{10}$$

Denote the closed ball of radius r centered at $\bar{x}_s$ in X by $B_{\bar{x}_s}(r) = \bar{x}_s + B(r)$, where

$$B(r) = \left\{ x \in X : \|x\|_X \leq r \right\} = \prod_{k=-2}^{\infty} \left[-\frac{r}{\omega_k^q}, \frac{r}{\omega_k^q} \right] = [-r, r]^3 \times \prod_{k=1}^{\infty} \left[-\frac{r}{k^q}, \frac{r}{k^q} \right]$$

is the closed ball of radius r centered at 0 in X. The idea is to introduce the radii polynomials to find (if possible) a uniform positive radius r so that for every $s \in \Delta$, $T_s : B_{\bar{x}_s}(r) \to B_{\bar{x}_s}(r)$ is a contraction. If such positive radius exists, then the operator $\widetilde{T} : \Delta \times B(r) \to B(r)$ defined by $\widetilde{T}(s, y) = T_s(y + \bar{x}_s) - \bar{x}_s$ is a uniform contraction. The Uniform Contraction Principle then yields a local chart within precise bounds given in terms of the radius r. The smoothness of the chart itself is a separate issue, and is dealt with later on in Section 2.3.

Recall the notation $x_{-2} = p_1$, $x_{-1} = p_2$ and $x_k = a_k$ for $k \geq 0$. Similarly, $[\mathcal{F}_s(x)]_{-2} = [\bar{\Phi}_s^T(x - \bar{x}_s)]_1$, $[\mathcal{F}_s(x)]_{-1} = [\bar{\Phi}_s^T(x - \bar{x}_s)]_2$ and $[\mathcal{F}_s(x)]_k = f_k(x)$ for $k \geq 0$. Define the uniform bounds $Y = (Y_k)_{k \geq -2}$ and $Z = Z(r) = (Z_k)_{k \geq -2}$ satisfying

$$\left| [T_s(\bar{x}_s) - \bar{x}_s]_k \right| \leq Y_k, \quad \forall\ s \in \Delta, \tag{11}$$

and

$$\sup_{b_1,b_2\in B(r)}\left|[DT_s(\bar{x}_s+b_1)b_2]_k\right| \le Z_k(r), \quad \forall\ s\in\Delta. \tag{12}$$

Lemma 2.2. *Consider $s\in\Delta$. If there exists an $r>0$ such that $\|Y+Z\|_X<r$, with Y and Z satisfying (11) and (12), respectively, then T_s is a contraction mapping on $B_{\bar{x}_s}(r)$ with contraction constant at most $\|Z\|_X/r<1$. Furthermore, there is a unique C^ℓ function $s\in\Delta\mapsto\tilde{x}(s)\in B_{\bar{x}_s}(r)$ such that $\mathcal{F}_s(\tilde{x}(s))=0$, and $\tilde{x}(s)$ lies in the interior of $B_{\bar{x}_s}(r)$ for all $s\in\Delta$.*

Proof. Fix an $s\in\Delta$ and consider $x,y\in B_{\bar{x}_s}(r)$ such that $x\neq y$. For sake of simplicity of the presentation, denote T_s by T. For any $k\ge -2$, the Mean Value Theorem implies

$$T_k(x)-T_k(y)=DT_k(z)(x-y)$$

for some $z=z(k)\in\{tx+(1-t)y\ :\ t\in[0,1]\}\subset B_{\bar{x}_s}(r)$. Note that $\frac{r(x-y)}{\|x-y\|_X}\in B(r)$. Thus from (12),

$$|T_k(x)-T_k(y)|=\left|DT_k(z)\frac{r(x-y)}{\|x-y\|_X}\right|\frac{1}{r}\|x-y\|_X\le\frac{Z_k(r)}{r}\|x-y\|_X, \tag{13}$$

and then

$$\|T(x)-T(y)\|_X\le\frac{\|Z(r)\|_X}{r}\|x-y\|_X.$$

Now, combining (12) and (13), one gets that $|T_k(x)-T_k(\bar{x}_s)|\le Z_k(r)$. Triangular inequality yelds

$$|T_k(x)-(\bar{x}_s)_k|\le|T_k(x)-T_k(\bar{x}_s)|+|T_k(\bar{x}_s)-(\bar{x}_s)_k|\le Z_k(r)+Y_k.$$

Therefore for any $x\in B_{\bar{x}_s}(r)$,

$$\|T(x)-\bar{x}_s\|_X=\sup_{k\ge-2}\{|T_k(x)-(\bar{x}_s)_k|\omega_k^q\}\le\sup_{k\ge-2}\{|Y_k+Z_k(r)|\omega_k^q\}=\|Y+Z(r)\|_X<r. \tag{14}$$

This proves that $T(B_{\bar{x}_s}(r))\subset B_{\bar{x}_s}(r)$. We can conclude that $T:B_{\bar{x}_s}(r)\to B_{\bar{x}_s}(r)$ is a contraction with contraction constant

$$\kappa\overset{\text{def}}{=}\frac{\|Z(r)\|_X}{r}<1. \tag{15}$$

Application of the Contraction Mapping Theorem on the Banach space $B_{\bar{x}_s}(r)$ gives the existence and uniqueness of a solution $\tilde{x}(s)$ of the equation $T_s(\tilde{x}(s))=\tilde{x}(s)$ in $B_{\bar{x}_s}(r)$, and therefore of $\mathcal{F}_s(\tilde{x}(s))=0$. From (14) we get that $\tilde{x}(s)$ is in the interior of $B_{\bar{x}_s}(r)$. As in Lemma 5 in [1], the operator $\widetilde{T}:\Delta\times B(r)\to B(r)$ defined by

$$\widetilde{T}(s,y)=T_s(y+\bar{x}_s)-\bar{x}_s$$

is a uniform contraction on Δ. Since $\mathcal{F}_s\in C^\ell(X,W)$, we have $\widetilde{T}\in C^\ell(\Delta\times B(r),B(r))$. By the Uniform Contraction Principle (e.g. see [14]), $\tilde{x}(s)$ is a C^ℓ function of $s\in\Delta$. □

Remark 2.3 (The computation of the Y and Z bounds). While, in practice, the Y bounds satisfying (11) can be obtained using interval arithmetic, the computation of the bound Z satisfying (12) is more delicate. In fact, the bound Z can be obtained as a polynomial bound in the variable radius r. More explicitly, the computation of the Z bound requires expanding each component of $DT_s(\bar{x}_s+b_1)b_2$ for all $b_1,b_2\in B_0(r)$. This is

equivalent to expanding each component of $DT_s(\bar{x}_s + \tilde{b}_1 r)\tilde{b}_2 r$ for all $\tilde{b}_1, \tilde{b}_2 \in B_0(1)$. If the nonlinearities of the original differential equation are polynomials of order less than or equal to n, then the operator f will consists of discrete convolutions with power at most n. Since $T_s(x) = x - A\mathcal{F}_s(x)$ and $DT_s(\bar{x}_s + \tilde{b}_1 r)\tilde{b}_2 r$, then each component of $DT_s(\bar{x}_s + \tilde{b}_1 r)\tilde{b}_2 r$ can be expanded as a polynomial of order n in r. While this computation can be performed using Taylor expansions, obtaining the sharpest bounds is still problem dependent and we refer to Section 5 for an explicit example. More generally, in the problem definition of Section 1, we assumed that the operator f is twice Fréchet differentiable, which insures that the Taylor expansion of $DT_s(\bar{x}_s + \tilde{b}_1 r)\tilde{b}_2 r$ will yield a quadratic polynomial in r.

Verifying in practice the hypotheses of Lemma 2.2 can be delicate. This is why we introduce the radii polynomials, which provide an efficient way to determine (when possible) the existence of a positive radius r such that the hypotheses of Lemma 2.2 are satisfied.

Before introducing the polynomials, we make two assumptions. Assume that there exists a number $M \geq m$, where m is the dimension of the finite dimensional projection $f^{(m)}$, such that the bounds Y and Z satisfying (11) and (12) are such that

A1. $Y_k = 0$ for all $k \geq M$.

A2. There exists a *uniform* polynomial bound $\tilde{Z}_M(r)$ such that, for all $k \geq M$,

$$Z_k(r) \leq \frac{\tilde{Z}_M(r)}{\omega_k^q}. \tag{16}$$

Before introducing the radii polynomials, let us make a few comments on assumptions **A1** and **A2**. If equation (1) comes from a problem involving polynomial nonlinearities, then the nonlinear terms in (1) are convolutions sums of the form $[\bar{a}^{(j_1)} * \bar{a}^{(j_2)} * \cdots * \bar{a}^{(j_\ell)}]_k$ which are eventually equal to zero for large enough k since $\bar{a}_k = 0$ for $k \geq m$. Hence, by construction of A defined in (9), and of the bound Y as in (11), there exists M such that Y_k can be defined to be 0 for $k \geq M$. Now, there are some analytic convolution estimates (e.g. the ones developed in [11, 13, 15]) that allow computing $\tilde{Z}_M(r)$ satisfying (16). These explicit estimates essentially follow from the fact that the Banach space Ω^q given in (4) is an algebra under discrete convolutions. The computation of the uniform polynomial bound $\tilde{Z}_M(r)$ is presented explicitly in the example of Section 5. We are now ready to define the radii polynomials.

Definition 2.4. Recall (11), (12) and (16). We define the finite radii polynomials $(p_k(r))_{k\geq -2}^{M-1}$ by

$$p_k(r) = Y_k + Z_k(r) - \frac{r}{\omega_k^q}, \quad k = -2, \ldots, M-1, \tag{17}$$

and the tail radii polynomial by

$$p_M(r) = \tilde{Z}_M(r) - r. \tag{18}$$

The following result justifies the construction of the radii polynomials of Definition 2.4.

Lemma 2.5. *If there exists $r > 0$ such that $p_k(r) < 0$ for all $k = -2, \ldots, M$, then there is a unique C^ℓ function $\tilde{x} : \Delta \to B_{\bar{x}_s}(r) : s \mapsto \tilde{x}(s)$ such that $\mathcal{F}_s(\tilde{x}(s)) = 0$, and $\tilde{x}(s)$ lies in the interior of $B_{\bar{x}_s}(r)$ for all $s \in \Delta$.*

Proof. For $-2 \leq k < M$, notice that $p_k(r) < 0$ implies that

$$\omega_k^q \big| Y_k + Z_k(r) \big| < r.$$

For $k \geq M$, since $Y_k = 0$ and $p_M(r) < 0$, we get that

$$\omega_k^q \big|Y_k + Z_k(r)\big| = \omega_k^q Z_k(r) = \tilde{Z}_M(r) < r.$$

Therefore we have

$$\|Y + Z\|_X = \sup_{k \geq -2} \omega_k^q \big|Y_k + Z_k(r)\big| < r.$$

The result then follows from Lemma 2.2. □

2.2 Construction of the bounds required for the radii polynomials

Recall the assumption that $f : \mathbb{R}^2 \times B_1 \to B_2$ is assumed to be twice Fréchet differentiable, that is $f \in C^\ell(\mathbb{R}^2 \times B_1, B_2)$, with $\ell \geq 1$.

While the explicit construction of the radii polynomials is problem dependent, we present a general way to construct them. For a more detailed example, we refer to Section 5, where the radii polynomials are explicitly defined and used to construct two-dimensional manifolds of equilibria of the Cahn-Hilliard equation. To compute $Y = (Y_k)_{k \geq -2}$ satisfying (11), we expand

$$T_s(\bar{x}_s) - \bar{x}_s = -A \begin{pmatrix} 0 \\ f(\bar{x}_s) \end{pmatrix}$$

as a polynomial in the variables s_1 and s_2 by using a Taylor expansion of order n_Y with $2 \leq n_Y \leq \ell$. For each $i, j \geq 0$ such that $2 \leq i + j \leq n_Y$ and for each $k \geq 0$, consider $y_k^{(i,j)} = y_k^{(i,j)}(\bar{x}_0, \bar{x}_1, \bar{x}_2)$ such that

$$f_k(\bar{x}_s) = f_k(\bar{x}_0) + s_1[f_x(\bar{x}_0)(\bar{x}_1 - \bar{x}_0)]_k + s_2[f_x(\bar{x}_0)(\bar{x}_2 - \bar{x}_0)]_k + \sum_{\substack{2 \leq i+j \leq n_Y \\ i,j \geq 0}} y_k^{(i,j)} s_1^i s_2^j. \quad (19)$$

From this, and using the fact that $|s_1|, |s_2| \leq 1$ for all $s = (s_1, s_2) \in \Delta$, consider bounds $Y_k^{(i,j)}$ such that $|y_k^{(i,j)}| \leq Y_k^{(i,j)}$. Therefore, set $Y_F = (Y_{-2}, Y_{-1}, \ldots, Y_{m-1})$ to be

$$Y_F = |A_m| \left(|f_F(\bar{x}_0)| + |[f_x(\bar{x}_0)(\bar{x}_1 - \bar{x}_0)]_F| + |[f_x(\bar{x}_0)(\bar{x}_2 - \bar{x}_0)]_F| + \sum_{\substack{2 \leq i+j \leq n_Y \\ i,j \geq 0}} Y_F^{(i,j)} \right). \quad (20)$$

From assumption **A1**, $Y_k = 0$ for all $k \geq M$, for some $M \geq m$. For more details on the existence of such M, we refer to the example in Section 5. For $m \leq k \leq M - 1$, set

$$Y_k = \frac{1}{|\mu_k|} \left(|f_k(\bar{x}_0)| + |[f_x(\bar{x}_0)(\bar{x}_1 - \bar{x}_0)]_F| + |[f_x(\bar{x}_0)(\bar{x}_2 - \bar{x}_0)]_F| + \sum_{\substack{2 \leq i+j \leq n_Y \\ i,j \geq 0}} Y_k^{(i,j)} \right). \quad (21)$$

As already mentioned in Remark 2.3, if the nonlinearities of the original problem are polynomials, then the nonlinearities of f will be discrete convolutions. In this case, all terms in (20) and (21) will be finite sums that can be evaluated using interval arithmetic.

We now turn to the computation of $Z(r) = (Z_k(r))_{k \geq -2}$ satisfying (12). To simplify the computation, define the linear operator $A^\dagger : X \to W$ by

$$(A^\dagger x)_k \stackrel{\text{def}}{=} \begin{cases} \left[D\mathcal{F}_0^{(m)}(\bar{x}_0) x_F \right]_k, & \text{if } -2 \leq k \leq m-1 \\ \mu_k x_k, & \text{if } k \geq m. \end{cases}$$

Consider $b_1, b_2 \in B(r)$ and expand

$$\begin{aligned} DT_s(\bar{x}_s + b_1)b_2 &= [I - A\,D\mathcal{F}_s(\bar{x}_s + b_1)]b_2 \\ &= [I - AA^\dagger]b_2 - A[D\mathcal{F}_s(\bar{x}_s + b_1)b_2 - A^\dagger b_2], \end{aligned}$$

where the first term is expected to be small, provided that A_m is a good approximate inverse for $D\mathcal{F}_0^{(m)}(\bar{x}_0)$. The idea is to compute a Taylor expansion of the other term $D\mathcal{F}_s(\bar{x}_s + b_1)b_2 - A^\dagger b_2$ in the variables s_1, s_2 and r. Choose a Taylor expansion of order n_Z with $2 \le n_Z \le \ell$. Let $b_1 = (p_1^{(1)}, p_2^{(1)}, a^{(1)})$ and $b_2 = (p_1^{(2)}, p_2^{(2)}, a^{(2)})$. Consider $\tilde{b}_1, \tilde{b}_2 \in B(1)$ such that $b_1 = \tilde{b}_1 r$ and $b_2 = \tilde{b}_2 r$, and denote $\tilde{b}_1 = (\tilde{p}_1^{(1)}, \tilde{p}_2^{(1)}, \tilde{a}^{(1)})$ and $\tilde{b}_2 = (\tilde{p}_1^{(2)}, \tilde{p}_2^{(2)}, \tilde{a}^{(2)})$. Then, consider $z_k^{(\ell,i,j)} = z_k^{(\ell,i,j)}(\tilde{b}_1, \tilde{b}_2, \bar{x}_0, \bar{x}_1, \bar{x}_2, \bar{\Phi}_0, \bar{\Phi}_1, \bar{\Phi}_2)$ such that

$$\begin{aligned} [D\mathcal{F}(\bar{x}_s + b_1)b_2 - A^\dagger b_2]_k &= [D\mathcal{F}(\bar{x}_s + \tilde{b}_1 r)\tilde{b}_2 r - A^\dagger \tilde{b}_2 r]_k \\ &= \sum_{\ell=1}^{n_Z} \left(\sum_{i=0}^{(n_Z+1-\ell)} \sum_{j=0}^{(n_Z+1-\ell-i)} z_k^{(\ell,i,j)} s_1^i s_2^j \right) r^\ell. \end{aligned} \tag{22}$$

Using the fact that for $s = (s_1, s_2) \in \Delta$, $|s_1|, |s_2| \le 1$ and $|(\tilde{b}_1)_k|, |(\tilde{b}_1)_k| \le \omega_k^{-q}$, consider bounds $Z_k^{(\ell)} = Z_k^{(\ell)}(\bar{x}_0, \bar{x}_1, \bar{x}_2, \bar{\Phi}_0, \bar{\Phi}_1, \bar{\Phi}_2)$ such that

$$\left| \sum_{i=0}^{(n_Z+1-\ell)} \sum_{j=0}^{(n_Z+1-\ell-i)} z_k^{(\ell,i,j)} s_1^i s_2^j \right| \le Z_k^{(\ell)}. \tag{23}$$

Then set $Z_F(r) = (Z_{-2}(r), \ldots, Z_{m-1}(r))$ to be

$$Z_F(r) = \left(\left| I - A_m D\mathcal{F}_0^{(m)}(\bar{x}_0) \right| \omega_F^{-q} \right) r + \sum_{\ell=1}^{n_Z} |A_m| Z_F^{(\ell)} r^\ell. \tag{24}$$

From assumption **A2** there exists a *uniform* polynomial bound $\tilde{Z}_M(r)$ such that, for all $k \ge M$, (16) is satisfied. For more details on the existence of such bound for an explicit problem, we refer to the example in Section 5. For $m \le k \le M-1$, set

$$Z_k(r) = \sum_{\ell=1}^{n_Z} \frac{1}{|\mu_k|} Z_k^{(\ell)} r^\ell. \tag{25}$$

Combining (20), (21), (24) and (25), we have all ingredients to construct the finite radii polynomials (16) from Definition 2.4.

We refer to Remark 2.3 for a comment about the computation of the Z bounds in general. This being said, even though the computation of the $z_k^{(\ell,i,j)}$ and Z_k^ℓ satisfying (22) and (23) is problem dependent and presented only in the example of Section 5, let us compute explicitly $z_k^{(1,1,0)}$, $z_k^{(1,0,1)}$ and $Z_k^{(1)}$, for $k \in \{-2, -1\}$.

2.2.1 Computation of $Z_k^{(1)}$, for $k \in \{-2, -1\}$.

Letting $\mathbf{k} \overset{\text{def}}{=} (-2, -1)$, note that

$$[D\mathcal{F}(\bar{x}_s + \tilde{b}_1 r)\tilde{b}_2 r - A^\dagger \tilde{b}_2 r]_{\mathbf{k}} = s_1 \left(\bar{\Phi}_1 - \bar{\Phi}_0\right)^T (\tilde{b}_2)_F r + s_2 \left(\bar{\Phi}_2 - \bar{\Phi}_0\right)^T (\tilde{b}_2)_F r.$$

Therefore,

$$z_{\mathbf{k}}^{(1,1,0)} = \left(\bar{\Phi}_1 - \bar{\Phi}_0\right)^T (\tilde{b}_2)_F \quad \text{and} \quad z_{\mathbf{k}}^{(1,0,1)} = \left(\bar{\Phi}_2 - \bar{\Phi}_0\right)^T (\tilde{b}_2)_F,$$

so that we can set the bound $Z_{\mathbf{k}}^{(1)} \in \mathbb{R}_+^2$ to be

$$Z_{\mathbf{k}}^{(1)} = \left|\left(\bar{\Phi}_1 - \bar{\Phi}_0\right)^T\right| \omega_F^{-q} + \left|\left(\bar{\Phi}_2 - \bar{\Phi}_0\right)^T\right| \omega_F^{-q}, \tag{26}$$

where $\omega_F^{-q} \stackrel{\text{def}}{=} (1, 1, 1, 1, \frac{1}{2^q}, \frac{1}{3^q}, \ldots, \frac{1}{(m-1)^q}) \in \mathbb{R}^{m+2}$.

2.3 Smoothness of the local chart

Suppose that we have computed numerical approximations $\bar{x}_0$, $\bar{x}_1$ and $\bar{x}_2$ corresponding to the simplex

$$\sigma \stackrel{\text{def}}{=} \bigcup_{s\in\Delta} \{\bar{x}_s\} \subset X.$$

Assume also that the hypotheses of Lemma 2.5 have been verified, yielding the existence of a set

$$\Sigma \stackrel{\text{def}}{=} \bigcup_{s\in\Delta} B_{\bar{x}_s}(r) \subset X$$

centered at the simplex σ, and containing a genuine solution chart $\tilde{x}(\Delta) \subset \Sigma \subset X$, where $\tilde{x}$ is a C^ℓ function such that $\mathcal{F}_s(\tilde{x}(s)) = 0$ for every $s \in \Delta$. We want to show that the local chart $\tilde{x}(\Delta)$ is C^ℓ smooth. For this we show that $\tilde{x}$ is a C^ℓ diffeomorphism. Since $\mathcal{F}_s(\tilde{x}(s)) = 0$ we get, in particular, that $\bar{\Phi}_s^T(\tilde{x}(s) - \bar{x}_s) = 0$ for every $s \in \Delta$. We have that

$$\begin{aligned}
\frac{\partial}{\partial s_1}\left(\bar{\Phi}_s^T(\tilde{x}(s) - \bar{x}_s)\right) &= \frac{\partial \bar{\Phi}_s^T}{\partial s_1}(\tilde{x}(s) - \bar{x}_s) + \bar{\Phi}_s^T \frac{\partial}{\partial s_1}(\tilde{x}(s) - \bar{x}_s) \\
&= (\Phi_1 - \Phi_0)^T(\tilde{x}(s) - \bar{x}_s) + \bar{\Phi}_s^T\left(\frac{\partial \tilde{x}}{\partial s_1} - (\bar{x}_1 - \bar{x}_0)\right) = 0.
\end{aligned}$$

Hence,

$$\bar{\Phi}_s^T \frac{\partial \tilde{x}}{\partial s_1}(s) = \bar{\Phi}_s^T(\bar{x}_1 - \bar{x}_0) - (\bar{\Phi}_1 - \bar{\Phi}_0)^T(\tilde{x}(s) - \bar{x}_s). \tag{27}$$

Similarly,

$$\bar{\Phi}_s^T \frac{\partial \tilde{x}}{\partial s_2}(s) = \bar{\Phi}_s^T(\bar{x}_2 - \bar{x}_0) - (\bar{\Phi}_2 - \bar{\Phi}_0)^T(\tilde{x}(s) - \bar{x}_s). \tag{28}$$

Define the matrix function $\mathcal{G}\colon \Delta \to \mathbb{R}^{2\times 2}$ by

$$\mathcal{G}(s) = \left(\bar{\Phi}_s^T \frac{\partial \tilde{x}}{\partial s_1}(s) \quad \bar{\Phi}_s^T \frac{\partial \tilde{x}}{\partial s_2}(s)\right). \tag{29}$$

The next result relates the fact that $\det(\mathcal{G})$ is non-vanishing on Δ to the smoothness of the local chart $\tilde{x}$ obtained from Lemma 2.5. Before, given any $\varepsilon > 0$, define the set Δ_ε to be the ε-neighbourhood of Δ, i.e.

$$\Delta_\varepsilon \stackrel{\text{def}}{=} \{s = (s_1, s_2) \mid s_1, s_2 \geq -\varepsilon \text{ and } s_1 + s_2 \leq 1 + \varepsilon\}. \tag{30}$$

Note that for any $\varepsilon \geq 0$, $\Delta \subset \Delta_\varepsilon$.

Lemma 2.6. *Let $\ell \geq 1$. Suppose that the hypotheses of Lemma 2.5 are satisfied, yielding the existence of a C^ℓ function $\tilde{x} : \Delta \to X$ such that $\mathcal{F}_s(\tilde{x}(s)) = 0$, for all $s \in \Delta$. Recall the definition of $\mathcal{G}$ in* (29)*. If*

$$\det(\mathcal{G}(s)) \neq 0, \quad \text{for all } s \in \Delta, \tag{31}$$

there exists $\varepsilon > 0$ such that $\tilde{x} : \Delta_\varepsilon \to \tilde{x}(\Delta_\varepsilon)$ is a C^ℓ diffeomorphism, with Δ_ε as in (30)*.*

Proof. By construction of the radii polynomials, there exists $\varepsilon_1 > 0$ such that the map $\tilde{x}$ extends to a C^ℓ function on Δ_{ε_1}. Now, $\tilde{x} \in C^\ell(\Delta)$ implies that $\det(\mathcal{G}) : \Delta \to \mathbb{R}$ is continuous. Hence, since $\det(\mathcal{G}) \neq 0$ on Δ, there exists $\varepsilon \in (0, \varepsilon_1)$ such that $\det(\mathcal{G}(s)) \neq 0$ for every $s \in \Delta_\varepsilon \subset \Delta_{\varepsilon_1}$. Hence, $\tilde{x} : \Delta_\varepsilon \to \tilde{x}(\Delta_\varepsilon)$ is a C^ℓ function. Since $\det(\mathcal{G}) \neq 0$ on Δ_ε, $\frac{\partial \tilde{x}}{\partial s_1}$ and $\frac{\partial \tilde{x}}{\partial s_2}$ are two linearly independent non trivial vectors in X. Hence, for any $s_0 \in \Delta_\varepsilon$, the operator

$$\frac{d\tilde{x}}{ds}(s_0) = \left[\frac{\partial \tilde{x}}{\partial s_1}(s_0) \quad \frac{\partial \tilde{x}}{\partial s_2}(s_0) \right] \tag{32}$$

is a bounded linear isomorphism of Δ_ε onto $\frac{d\tilde{x}}{ds}(s_0)(\Delta_\varepsilon)$. Then, by the Inverse Function Theorem, there exists an open neighbourhood V_{s_0} of $\tilde{x}(s_0)$ in $\frac{d\tilde{x}}{ds}(s_0)(\Delta_\varepsilon) \subset X$ and a *local* C^ℓ inverse function $\tilde{x}_{s_0}^{-1} : V_{s_0} \to \Delta_\varepsilon$ such that $\tilde{x}_{s_0}^{-1} \circ \tilde{x}$ is the identity on V_{s_0}. Since, $\tilde{x}(\Delta_\varepsilon) \subset \cup_{s_0 \in \Delta_\varepsilon} V_{s_0}$, we can define a C^ℓ inverse function $\tilde{x}^{-1} : \tilde{x}(\Delta_\varepsilon) \to \Delta_\varepsilon$. □

Having computed a simplex σ given by three numerical approximations $\bar{x}_0$, $\bar{x}_1$, $\bar{x}_2$ and their respective kernels $\bar{\Phi}_0$, $\bar{\Phi}_1$, $\bar{\Phi}_2$, the rigorous computation of a local smooth chart of the manifold goes as follows: compute the radii polynomials using interval arithmetic, verify the hypotheses of Lemma 2.5 and finally verify the smoothness hypothesis (31) with interval arithmetic. We will refer to this procedure as "*rigorous verification*" (or simply "*verification*") of the simplex σ. Section 3 shows how we compute a simplicial approximation (triangulation) of the implicitly defined manifold. Then, the results in Section 4 yield an atlas which shows that what we actually computed is a smooth C^ℓ manifold.

3 Multi-parameter continuation algorithm

As already mentioned, our method relies on the ability to compute a simplicial approximation (triangulation) of a portion of a two-dimensional manifold implicitly defined by an infinite dimensional nonlinear equation on X. In order to carry out the computations, a finite dimensional projection must first be considered. This means that, in practice, we need to compute a triangulation of a manifold $\mathcal{M}$ embedded in $\mathbb{R}^n$:

$$\mathcal{M} \subset \{x \in \mathbb{R}^n : \ F(x) = 0, \text{ with } F : \mathbb{R}^n \to \mathbb{R}^{n-2}\},$$

where we typically think of F as being one realization of the map $f^{(m)}$ defined in Section 2, for some $m \in \mathbb{N}$. For sake of simplicity of the presentation, we use the same notation $\mathcal{M}$ to denote the manifold embedded in $\mathbb{R}^n$ and the manifold embedded in the infinite dimensional Banach space X. In addition to that, when describing the algorithm for the numerical computation of a simplicial approximation of $\mathcal{M}$, we will not distinguish between rigorous mathematical statements and statements that are only "numerically true". For example, we may write $x \in \mathcal{M}$, but mean that we numerically compute x to be approximately in $\mathcal{M}$.

There is a considerable amount of literature devoted to the numerical continuation of multidimensional manifolds implicitly defined by nonlinear equations. The methods that have been proposed essentially fall into two classes: simplicial methods (e.g. see [10] and references therein) and predictor-corrector methods (see [6, 7, 8, 16]). Predictor-corrector

methods show more favorable computational complexity in the case of low dimensional manifolds embedded in a high dimensional space, which is the case of interest for us. Moreover, they are more prone to the implementation of adaptive strategies based on local properties of the manifold. From our standpoint, the main feature that distinguishes among the predictor-corrector methods cited above is how the manifold is represented. In [6], the manifold is represented as a set of overlapping neighborhoods, each defined through a chart, a center point, basis for the tangent space at the center point, and other relevant data. A triangulation of the manifold can be constructed *a posteriori* by appropriately connecting the center points of the neighborhoods, but this does not allow for adaptive construction of the triangulation. In [7, 8, 16] the manifold is represented as a database of nodes and simplices. The database is progressively built by adding one simplex at a time. This does allow for appropriate evaluation of each simplex before it is actually added to the database, which will be an essential feature of the method we propose (see Section 3.1.3).

For these reasons, we decided to build our algorithm upon the one proposed by Brodzik and Rheinboldt in [8]. Even though the main philosophy of their algorithm is essentially intact, yet we introduce several novelties that improve its robustness and make it suitable for our purpose, as described in the remark below.

Remark 3.1. The main differences between our approach and the one from Brodzik and Rheinboldt in [8] are: (1) adaptive step-size selection based on the outcome of the verification test; (2) check for non-local overlap of simplices; (3) a sorting rule on the "frontal nodes" aimed at limiting the computational complexity of the aforementioned check; (4) simplicial neighborhoods allowed to have more than six simplices.

We now give a general description and some implementation details of the algorithm we use to perform our task, putting particular emphasis on the novelties while passing over some implementation details, for which we refer the reader to [8].

3.1 Description of the algorithm

Under suitable assumptions on DF, the solution set $\{x \in \mathbb{R}^n : \ F(x) = 0\}$ is a (collection of) smooth manifold(s). We are interested in computing a triangulation of the portion of the solution set that lies inside a given bounded region B of $\mathbb{R}^n$.

3.1.1 Constructing the first patch

As is typical of all continuation techniques, the algorithm starts off by considering an initial, user supplied, *node* $x_0 \in \mathcal{M} \cap B$, and then proceeds to explore the manifold from there. An initial regular hexagonal neighborhood centered at x_0 on the tangent plane $\mathcal{T}_{x_0}\mathcal{M}$ is considered, where each vertex v_i, $i = 1, \ldots, 6$, of the hexagon is taken at a user supplied distance h_0 from x_0. Each of the six vertices of the hexagon is then projected onto $\mathcal{M}$ orthogonally to $\mathcal{T}_{x_0}\mathcal{M}$, see Figure 1. The projection is done via a stationary Gauss-Newton method. For $x^{(0)} = v_1, \ldots, v_6$, we iterate

$$x^{(k+1)} = x^{(k)} - DF(x_0)^+ F(x^{(k)}), \quad k = 0, 1, \ldots \tag{33}$$

until convergence, where $DF(x_0)^+ = DF(x_0)^T \left(DF(x_0)DF(x_0)^T\right)^{-1}$ is the Moore-Penrose pseudoinverse of $DF(x_0)$. Details and convergence properties of Gauss-Newton's method are in [17]. We declare successful convergence when

$$\left\| x^{(k+1)} - x^{(k)} \right\| < \texttt{tol} \left(1 + \left\| x^{(0)} \right\|\right)$$

within a prescribed number iterations. In all of our computations, we have chosen `tol` $= 10^{-12}$. The implementation follows closely the one adopted in [8] and [16]. Let

$$DF(x_0)^T = \begin{bmatrix} Q_1 & Q_2 \end{bmatrix} \begin{bmatrix} R \\ 0 \end{bmatrix} \tag{34}$$

be a QR factorization of $DF(x_0)^T$, with $Q_1 \in \mathbb{R}^{n\times(n-2)}$ and $Q_2 \in \mathbb{R}^{n\times 2}$ having mutually orthonormal columns, and $R \in \mathbb{R}^{(n-2)\times(n-2)}$ being upper triangular. As already mentioned in Section 2, $DF(\cdot)$ will always be assumed to be full rank at each computed node on $\mathcal{M}$. In particular, $DF(x_0)$ is full rank, which implies that R is invertible. Then the iterations (33) are implemented as follows:

$$\text{solve } Rz^{(k)} = F(x^{(k)}), \quad \text{set } x^{(k+1)} = x^{(k)} - Q_1 z^{(k)}, \quad k = 0, 1, \ldots \tag{35}$$

Note that the columns of Q_2 form an orthonormal basis for $\ker(DF(x_0))$, which spans $\mathcal{T}_{x_0}\mathcal{M}$. This also justifies the assertion that the iterates in (35) proceed in the direction perpendicular to $\mathcal{T}_{x_0}\mathcal{M}$. The computation of the decomposition in (34) will be our only source of orthonormal bases for tangent spaces.

If projection fails for a vertex v_i, its distance from x_0 is reduced by a fixed factor $\tau > 1$ (i.e. h is replaced by h/τ) and projection is reattempted until convergence is successful or a minimum distance $h_{\min}$ is reached. In all our computations, we have set $\tau = 1.2$.

Assuming successful convergence for all the six vertices, six simplices and six new nodes have been computed. Before they are added to the database, each simplex needs to be checked for *verification* as specified in Section 3.1.3. If verification fails, the two edges of the simplex that are connected to x_0 are shortened again by τ and the test is reattempted until it is successful or $h_{\min}$ is reached. Assuming successful outcome of the test on each simplex, the simplices are added to the database and declared *verified* by setting an appropriate flag to true, see Section 3.1.6. Upon being added to the database, each node is marked as *interior* if it belongs to B, *exterior* otherwise. Among interior nodes, those that lie on the boundary of the portion of $\mathcal{M}$ that still needs to be explored are marked as *frontal*. Simplices that are incident to a frontal node will also be referred to as *frontal*.

At this stage the database contains six simplices and seven nodes, and, typically, all nodes except x_0 are expected to be frontal. The six simplices constitute the first *patch*[1] of the triangulation. The algorithm now proceeds via an advancing front technique.

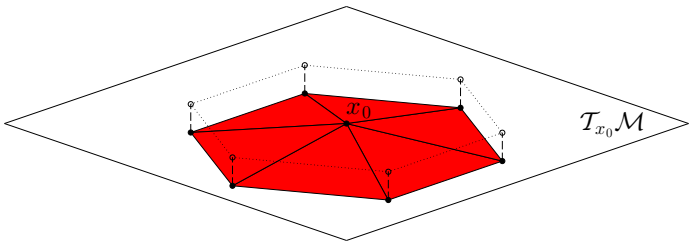

Figure 1: First patch.

[1]By "patch centered at x" we mean the neighborhood of simplices adjacent to x.

3.1.2 Advancing the front

Let $\mathcal{Q}$ be the (non-empty) set of all frontal nodes at a given stage. The algorithm will now select a node in $\mathcal{Q}$ according to a given sorting rule (we will elaborate on this in Section 3.1.4), and attempt to complete its patch. Suppose that the frontal node x_c is picked. The algorithm will now try to fill in the patch centered at x_c with the missing simplices.

First, the existing simplices that are adjacent to x_c are projected orthogonally on the tangent plane $\mathcal{T}_{x_c}\mathcal{M}$. To do so, we compute the QR factorization of $DF(x_c)$ as in (34), and then project their incident nodes on $\mathcal{T}_{x_c}\mathcal{M}$ using the orthogonal projector $P = Q_2 Q_2^T$. Then the *gap angle* γ is computed. The gap angle γ is defined as the "exterior" angle, on $\mathcal{T}_{x_c}\mathcal{M}$, formed by the two (projected) extremal edges of the incomplete patch, see Figure 2a. To compute it, we used the algorithm described in [7].

If the gap angle is too small (i.e., below a user defined threshold $\gamma_{\min}$) the two extremal simplices of the patch are glued together by "identifying" their closer edges. Let $e_1 = \{x_c, x_1\}$ and $e_2 = \{x_c, x_2\}$ be the two edges under consideration. In practice, this operation is performed by simply projecting on $\mathcal{M}$ the point $\bar{x} = \frac{1}{2}(x_1 + x_2)$, identifying x_1 and x_2 with $\bar{x}$, and appropriately updating the adjacency relations in the database. Since this operation modifies one node for each of the simplices involved, the corresponding verification flags are set to false. In all our experiments, we set $\gamma_{\min} = \pi/6$.

Assume γ is above $\gamma_{\min}$. The number k of new simplices that need to be added to complete the patch centered at x_c is determined as follows:

$$k = \min\left\{1, \left[\frac{\gamma}{\pi/3}\right]\right\}, \tag{36}$$

with the added requirement that the total number of simplices that compose a patch cannot exceed a prescribed number (which we chose equal to ten). Here $[y]$ denotes the nearest integer to y. Note that, through the use of formula (36), we aim at simplices whose angle adjacent to x_c is as close as possible to $\pi/3$.

Suppose $k > 1$. This means that $k-1$ new nodes need to be computed to complete the patch. We consider the $k-1$ half-lines on $\mathcal{T}_{x_c}\mathcal{M}$ that divide γ into k equal parts, see Figure 2a. Along each direction, we form the predictors x_i^{pred}, $1 \le i \le k-1$, at distance h from x_c. The step-size h is chosen as follows: it is the length of the shorter edge adjacent to x_c already in the database, multiplied by the factor τ. All the predictors are consecutively projected onto $\mathcal{M}$ via the same method described in Section 3.1.1. If a projection fails, the step-size h is reduced by the factor τ (again, just as in Section 3.1.1) and projection is reattempted for all the predictors, until convergence is successful or $h_{\min}$ is reached. Assuming all projections are successful with the common step-size h, let x_i, $1 \le i \le k-1$, be the projected points. These are, potentially, the $k-1$ new nodes that identify the k missing simplices. Whether or not they will be incorporated into the database depends on the outcome of the verification. Each of these simplices is checked for verification. If verification is successful, we proceed to the next stage. If verification fails on a simplex, the simplex is rejected. The two edges of the rejected simplex that are incident to x_c are "shortened" again by τ, and verification is reattempted until it is successful or $h_{\min}$ is reached. Note that shortening of an edge is performed keeping the node x_c fixed; this causes the other node incident to the edge to detach from $\mathcal{M}$, and triggers its re-projection onto $\mathcal{M}$. If any previously verified simplex was altered (i.e., one of its nodes was modified), the corresponding verification flag is set to false.

If $k = 1$, there is no need to compute new nodes. The simplex identified by the two extremal edges of the incomplete patch will complete the patch. If it passes verification, we proceed to the next stage. In case it fails, the simplex is handled just as described above.

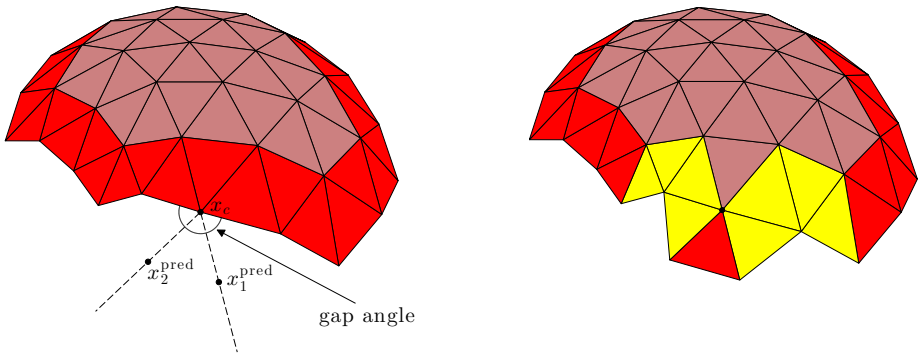

(a) Computation of the predictors.

(b) Patch completed.

Figure 2: Advancing the front: general step. Frontal simplices are colored in red. Incomplete patches centered at priority frontal nodes are colored in yellow.

Assuming successful verification, each simplex is checked for overlap with any of the currently frontal simplices (see Section 3.1.5). The current version of the algorithm halts if overlap is detected. Correct handling of this situation is ongoing work, and we anticipate it will be a feature of a next version.

Finally, having ruled out overlap, all newly created simplices and nodes are added to the database, with all simplices flagged as verified. Nodes are declared interior/exterior/frontal as specified in Section 3.1.1.

We recall that we heuristically set $\tau = 1.2$. In our experiments, this choice produced a nearly optimal balance between two goals: minimizing the number of rejections and maximizing the average surface area of a simplex.

The simplices (if any) that, during the process described above, had their verification flag set to false (due to alteration of one of their nodes) undergo the verification test again. In case the verification test fails, we split the simplex in four new sub-simplices by appropriately connecting the nodes of the original simplex and the mid-points of its edges (see Figure 3), and then apply the verification test to each one of these new simplices. This is done only at the level of the simplex, that is, the mid-points are not projected to the manifold. In case the verification for some of these sub-simplices fails, any failing sub-simplex undergoes the splitting process again. The process is repeated until either all the sub-simplices are verified or a maximum number of subdivisions is reached. If the verification is successful before the maximum number of subdivisions allowed is reached, the original simplex is declared as verified and the sub-simplices are discarded. If the maximum number of subdivision is reached the computation is halted.

Remark 3.2 (**Reasons why the splitting process may fail).** It is important to remark that we assume that the solution manifold is regular as described in the Problem Definition in Section 1. Recall that this assumption is that for all $x \in \mathcal{M}$, the linear operator $Df(x) : \mathbb{R}^2 \times B_1 \to B_2$ has a bounded inverse. However, in practice, we may not know a priori that the manifold is regular, and therefore, the verification could fail because one of the following two situations occurs.

1. The manifold $\mathcal{M}$ is regular over a given simplex $\sigma \in \mathcal{S}$, but it varies too much over σ. In this case, with a large enough number of subdivisions we will be able to verify the manifold.

2. There is a singular point in the manifold over a given simplex $\sigma \in \mathcal{S}$. In this situation, the splitting process will fail regardless of how many subdivisions of σ we take.

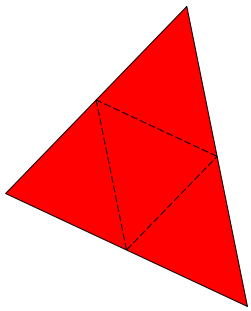

Figure 3: Splitting of a simplex.

In our experiments, successful verification of a simplex turned out to be a much stricter requirement than successful projection of predictors, so much that we can assert that, in practice, the step-size selection strategy of our algorithm is solely driven by the verification.

3.1.3 Verification of a simplex

Let $S = \{x_1, x_2, x_3\}$ be a newly computed simplex. Before adding it to the database, we need to rigorously verify, using interval arithmetic, the hypothesis of Lemmata 2.5 and 2.6. We refer to this procedure as *rigorous verification* (or simply *verification*), which is a test providing precise bounds in the Banach space X around an approximate simplex within which a genuine smooth local chart of the manifold is rigorously guaranteed to exist. We refer to Section 2 for details. In order to carry out the verification, the matrices $\bar{\Phi}_i \in \mathbb{R}^{n\times 2}$, $i = 1, 2, 3$, introduced in Section 2, need to be available; we recall that each $\bar{\Phi}_i \in \mathbb{R}^{n\times 2}$ must have orthonormal columns that span the kernel of $DF(x_i)$. In practice, each matrix is computed as follows.

Let Φ_{ref} be a matrix whose columns form an orthonormal basis for $\mathcal{T}_{x_0}\mathcal{M}$, where we recall that x_0 is the first node considered on the triangulation. First, an orthonormal basis ϕ_1^i, ϕ_2^i for $DF(x_i)$ is computed through the decomposition in (34). Let $\Phi_i = [\phi_1^i, \phi_2^i]$. Then, Φ_i is "rotated" as close as possible to Φ_{ref} through the "moving frame" algorithm adopted by Rheinboldt in [16], which renders a matrix $Q \in \mathbb{R}^{2\times 2}$, $Q^TQ = I$, such that $\|\Phi_i Q - \Phi_{\text{ref}}\|_{\text{F}}$ is minimized, where $\|\cdot\|_{\text{F}}$ denotes the Frobenius norm of a matrix. Finally, we set $\bar{\Phi}_i = \Phi_i Q$. Of course, we only run this procedure if x_i was a newly computed node, not yet in the database. Otherwise, we simply obtain the frame from the database, see Section 3.1.6.

As proved in [16], as far as the range of Φ_{ref} induces a coordinate system on the portion of $\mathcal{M}$ under interest, this procedure is guaranteed to produce frames $\bar{\Phi}_i$ that vary smoothly with respect to the node x_i. Motivation for using this procedure comes solely from the aim to limit the magnitude of the first two coefficients in Table 4, and therefore increase the chances of successful verification of a simplex.

3.1.4 Sorting the queue of frontal simplices

The way the queue of frontal nodes is visited is critical to the complexity of the procedure described in Section 3.1.5, which grows proportionally to the number of frontal simplices.

This consideration has lead us to implement the sorting strategy that is described below.

Upon completion of a new patch (with the exemption of the first patch), we compute the gap angle at the two "extremal" new frontal nodes, i.e. those that also belong to a simplex external to the patch. If the gap angle is below a given threshold γ_{prio}, the corresponding node is declared a *priority node* and the computed gap angle is saved in the database. In all our computations, we have chosen $\gamma_{\text{prio}} = 5\pi/6$, which is equivalent to giving priority to nodes whose completion of the patch needs two or less simplices. See Figure 2b. When picking a new node from the set $\mathcal{Q}$ of frontal nodes, precedence is given to priority nodes. In case there are more than one priority nodes, we pick first the node that has the smallest gap angle.

Besides limiting the size of the set of frontal simplices, this strategy has proven successful also in growing the triangulation, loosely speaking, in a convex fashion, avoiding the formation of "tentacles" that may cause artificial overlaps.

3.1.5 Checking for overlap

Before adding a newly created simplex to the database, one needs to verify that it does not overlap with the portion of manifold that has already been triangulated. Failure to do so may cause the algorithm to cover the same portion of the manifold more than once, and even enter an infinite loop.

To detect this situation we have implemented a procedure based on the Separation Theorem for convex sets [18]: any two disjoint compact convex sets in $\mathbb{R}^n$ are strictly separated by a hyperplane. In particular, any two non-overlapping triangles on the plane are separated by a line. It is easy to see that, in order to check whether two given triangles on the plane overlap, it is enough to test each of the six lines that contain an edge of one triangle as follows: if any of those lines separates the vertex that belongs to the same triangle from the three vertices that belong to the other, then the triangles do not overlap; if this separation test fails for all the six lines, the triangles do overlap.

Our strategy to check for overlap of two simplices is an adaptation of the idea described above to our context. Given two simplices T_1 and T_2, we perform the following *separation test*:

1. (a) project T_2 orthogonally on the 2-dimensional plane H determined by T_1; Call $\tilde{T}_2$ the projected simplex;
   (b) for each line $l \subset H$ that contains an edge of T_1, check whether l separates the vertex of T_1 exterior to l from all the vertices of $\tilde{T}_2$; in practice, the check is performed projecting each vertex on a line (*separating axis*) $l^\perp \subset H$ perpendicular to l, see Figure 4; if l separates T_1 and $\tilde{T}_2$, declare T_1 and T_2 not overlapping and leave the test;
2. repeat part 1. exchanging the roles of T_1 and T_2;
3. if parts 1. and 2. have not revealed the existence of a separating line, declare T_1 and T_2 overlapping.

Before being added to the database of simplices, each newly created (and verified) simplex is checked for overlap against all the frontal simplices currently in the database. It is enough to consider only frontal simplices, as intersection with a non-frontal simplex is ruled out by successful outcome of the verification. The separation test may produce false negatives: clearly, the fact that T_1 and $\tilde{T}_2$ overlap does not necessarily imply that T_1 and T_2 do so. In order to reinforce the test, we do as follows. In case of lack of separating line, a

proximity check is also performed: T_1 and T_2 are declared not-overlapping if their distance is larger then 10 times the length of the longest edge.

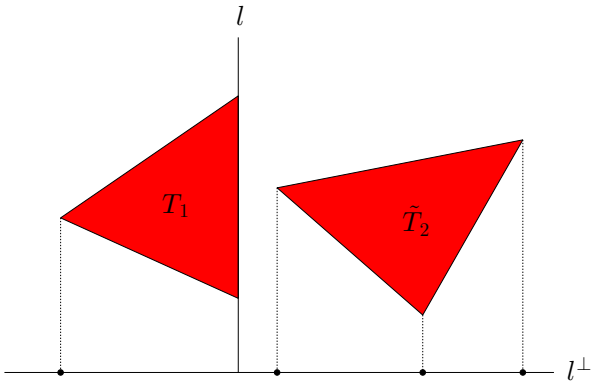

Figure 4: Separation test; the two triangles are intended to lie on the plane H.

3.1.6 The database

The database is made of two structure arrays, named `node` and `simplex`. Each array consists of several cell arrays that contain the relevant data of the triangulation, as shown in the Tables 1 and 2. The k-th element of each array contains data that are relevant to the k-th node, or simplex.

name	content
`node.coord`	coordinates (n-dimensional column vector)
`node.type`	node type; it's an integer k that indicates one of the following: interior ($k = 0, 1$), exterior ($k = 2$), frontal without priority ($k = -1$), frontal with priority ($k = -2$)
`node.simplex`	indices of incident simplices
`node.frame`	orthonormal basis for the tangent space ($n \times 2$ matrix with mutually orthonormal columns)
`node.gap`	gap angle (non-empty only for priority nodes)

Table 1: Structure array of nodes

name	content
`simplex.node`	indices of the incident nodes
`simplex.verified`	verification flag; 1 (true) if the simplex was successfully verified, 0 (false) otherwise

Table 2: Structure array of simplices

We point out that the orthonormal frames in `node.frame` are saved (and, if necessary, updated) only when a simplex incident to the corresponding node is successfully verified. We always make sure that two adjacent simplices that passed verification did so sharing exactly the same data (coordinates and orthonormal frames for the tangent space) at the common nodes. This is key in going from computing the local charts to obtaining a globally smooth atlas of the manifold, as will be explained in Section 4.

4 Rigorous computation of the global manifold

In Section 2 we show how to rigorously construct local smooth charts. In this section we describe how these charts fit together to form a smooth manifold $\mathcal{M}$. Suppose that we have computed, as described in Section 3, a simplicial approximation $\mathcal{S}$ for a portion of the solution set $\{x \in X : f(x) = 0\}$. For each simplex $\sigma \in \mathcal{S}$ assume that we have verified the hypotheses of Lemmas 2.5 and 2.6, and therefore we have a map $\tilde{x}_\sigma \colon \Delta \to X$ such that $\mathcal{F}_s(\tilde{x}_\sigma(s)) = 0$ for all $s \in \Delta$, where we recall that $\Delta = \{s = (s_1, s_2) \mid s_1, s_2 \geq 0 \text{ and } s_1 + s_2 \leq 1\}$. By Lemma 2.6 there is an $\varepsilon = \varepsilon(\sigma) > 0$ such that $\tilde{x}_\sigma$ can be extended to a C^ℓ diffeomorphism, also denoted by $\tilde{x}_\sigma$, on $\Delta_\varepsilon \stackrel{\text{def}}{=} \{s = (s_1, s_2) \mid s_1, s_2 \geq -\varepsilon \text{ and } s_1 + s_2 \leq 1 + \varepsilon\}$. For each $\sigma \in \mathcal{S}$, let $U_\sigma = \tilde{x}_\sigma(\Delta_\varepsilon)$ and define

$$\mathcal{M} \stackrel{\text{def}}{=} \bigcup_{\sigma \in \mathcal{S}} U_\sigma \,, \tag{37}$$

then U_σ are *charts* and $\tilde{x}_\sigma^{-1}$ are *chart maps* for $\mathcal{M}$. Hence $\mathcal{M}$ is a *two-dimensional manifold*. To show that $\mathcal{M}$ is a smooth manifold essentially all we have to show is that the local charts are smooth along the edges of adjacent simplices.

First we show that we have a connected manifold. When computing the local charts for two adjacent simplices, we want to make sure that the charts agree on the common edge. Since the charts are the zeros of $\mathcal{F}_s(x)$ given by (8), we need to construct the functions $\mathcal{F}_s(x)$ in such a way that they agree along the common edges of adjacent simplices. Recalling that the function $\mathcal{F}_s(x)$ is constructed for each simplex in terms of its vertices $\bar{x}_i$ and the kernels $\bar{\Phi}_i$ at the vertices, we need to make sure that the kernel used in each vertex is the same for all simplices that share that vertex. For this reason, when computing the simplicial approximation $\mathcal{S}$, we compute and store one kernel for each vertex and perform the proofs using these kernels. By doing so, the equations we solve on any two adjacent simplices agree on the common edge, and we have a connected manifold.

In Theorem 4.2, we will prove that we have a smooth manifold. In order to do so, we need the following lemma.

Lemma 4.1. *Suppose that the hypotheses of Lemma 2.5 are satisfied, yielding the existence of a C^ℓ function $\tilde{x} : \Delta \to X$ such that $\mathcal{F}_s(\tilde{x}(s)) = 0$, for every $s \in \Delta$. Then the linear operator $D\mathcal{F}_s(\tilde{x}(s))$ is invertible for every $s \in \Delta$.*

Proof. Given $s \in \Delta$, since $\tilde{x}(s) \in B_{\bar{x}_s}(r)$, there exists $b_0 = b_0(s) \in B(r)$ such that $\tilde{x}(s) = \bar{x}_s + b_0$. Hence, for every k, every $s \in \Delta$ and $u \in B(1)$,

$$\Big|[DT_s(\tilde{x}(s))u]_k\Big| r = \Big|[DT_s(\bar{x}_s + b_0)u]_k\Big| r \leq \sup_{b_1, b_2 \in B(r)} \Big|[DT_s(\bar{x}_s + b_1)b_2]_k\Big| \leq Z_k(r).$$

Therefore, recalling (15), the operator norm of $DT_s(\tilde{x}(s))$ in X satisfies

$$\|DT_s(\tilde{x}(s))\|_X = \sup_{u \in B(1)} \|DT_s(\tilde{x}(s))u\|_X \leq \frac{\|Z\|_X}{r} < 1. \tag{38}$$

Recalling the definition of T_s in (10), $DT_s(\tilde{x}(s)) = I - A\,D\mathcal{F}_s(\tilde{x}(s))$. From (38), the Neumann series of $DT_s(\tilde{x}(s))$ converges in the operator norm $\|\cdot\|_X$, and hence we have that the operator $A\,D\mathcal{F}_s(\tilde{x}(s)) = I - DT_s(\tilde{x}(s))$ is invertible. Therefore, $D\mathcal{F}_s(\tilde{x}(s))$, restricted to its image, is invertible. □

We now show that we have a smooth manifold. This means, in particular, that we can define a tangent plane at every point of the manifold. In other words, the manifold does not have any sharp points.

Theorem 4.2. *$\mathcal{M}$ is a C^ℓ manifold.*

Proof. We have from Lemma 2.6 that the chart maps $\tilde{x}_\sigma^{-1}$ are C^ℓ diffeomorphisms. To show that $\mathcal{M}$ is a C^ℓ manifold, we need to show that the local charts are smooth along the edges of adjacent simplices. Suppose then that we have two local charts corresponding to two adjacent simplices. More precisely, assume that we have two C^ℓ functions $\tilde{x}^{(i)}\colon \Delta_{\varepsilon(\sigma_i)} \to X$, for $i = 1, 2$, corresponding to adjacent simplices σ_1 and σ_2, such that $\tilde{x}^{(i)}(s)$ is the unique solution of

$$\mathcal{F}_s^{(i)}(x) = \begin{pmatrix} {\Phi_s^{(i)}}^T(x - x_s^{(i)}) \\ f(x) \end{pmatrix}$$

in a set $B_{x_s^{(i)}} \subset X$ for every $s \in \Delta$. Since σ_1 and σ_2 share a common edge, we can assume, without loss of generality, that the common solution *along this common edge* is parametrized by $\tilde{x}^{(1)}_{(s_1,0)} = \tilde{x}^{(2)}_{(s_1,0)}$, with $s_1 \in [0,1]$. Define $g : \Delta_\varepsilon \to X$ by

$$g(s_1, s_2) = \mathcal{F}^{(1)}_{(s_1,s_2)}(\tilde{x}^{(2)}(s_1, s_2)).$$

Then, for every $s_1 \in [0,1]$, $g(s_1, 0) = \mathcal{F}^{(1)}_{(s_1,0)}(\tilde{x}^{(2)}(s_1, 0)) = 0$. Since $\tilde{x}^{(2)}$ is C^ℓ on Δ_ε, $g(s_1, 0)$ is C^ℓ on $(-\varepsilon, 1+\varepsilon)$, which means that we can compute $\frac{\partial g}{\partial s_1}(s_1, 0)$ for $s_1 \in [0,1]$. For each $s_1 \in [0,1]$ we get

$$\frac{\partial g}{\partial s_1}(s_1, 0) = D_x\mathcal{F}^{(1)}_{(s_1,0)}(\tilde{x}^{(2)}(s_1, 0))\frac{\partial \tilde{x}^{(2)}}{\partial s_1}(s_1, 0).$$

From the proof of Lemma 2.6, the vector $\frac{\partial \tilde{x}^{(2)}}{\partial s_1}(s_1, 0)$ is nontrivial for each $s_1 \in [0,1]$. From Lemma 4.1, $D_x\mathcal{F}^{(1)}_{(s_1,0)}(\tilde{x}^{(1)}(s_1, 0)) = D_x\mathcal{F}^{(1)}_{(s_1,0)}(\tilde{x}^{(2)}(s_1, 0))$ is invertible. Hence, we get that the vector $\frac{\partial g}{\partial s_1}(s_1, 0)$ is nontrivial for each $s_1 \in [0,1]$. Then, for a given $s_1 \in [0,1]$, we can use the Implicit Function Theorem to conclude that there exists $\varepsilon_2 > 0$ such that $g(s_1, s_2) = \mathcal{F}^{(1)}_{(s_1,s_2)}(\tilde{x}^{(2)}(s_1, s_2)) = 0$ for each $s_2 \in [-\varepsilon_2, \varepsilon_2]$, and that $\tilde{x}^{(2)} \in C^\ell([0,1] \times [-\varepsilon_2, \varepsilon_2])$. Therefore, $\tilde{x}^{(2)} : [0,1] \times [-\varepsilon_2, \varepsilon_2] \to X$ glues C^ℓ smoothly the solutions $\tilde{x}^{(1)}$ and $\tilde{x}^{(2)}$.

Since the chart maps $\tilde{x}_\sigma^{-1}$ are C^ℓ diffeomorphisms and they are also C^ℓ smooth along the edges of adjacent simplices, $\mathcal{M}$ is a C^ℓ manifold. □

5 Two-dimensional manifold of equilibria of Cahn-Hilliard

Consider the Cahn-Hilliard equation

$$\begin{cases} u_t = -(\varepsilon^2\Delta u + u - u^3)_{yy}, & \text{in } [0,1] \\ u_y = u_{yyy} = 0, & \text{for } y = 0, 1 \end{cases} \tag{39}$$

defined on the interval domain $[0,1] \subset \mathbb{R}$, where $u = u(y,t)$ and $\varepsilon > 0$ models interaction length. Equation (39) was introduced in [19] as a model for phase separation in binary alloys. The model is mass preserving, meaning that, for any solution u, the total mass $\sigma \stackrel{\text{def}}{=} \int_0^1 u(y,t)dy$ remains constant for all $t \geq 0$. Doing a change of coordinates $\lambda \stackrel{\text{def}}{=} 1/\varepsilon^2 > 0$, the equilibria of (39) are given by the solutions of the elliptic boundary value problem

$$\begin{cases} \frac{1}{\lambda} u_{yy} + u - u^3 = c, & \text{in } [0,1] \\ u_y = 0, & \text{for } y = 0, 1 \end{cases} \tag{40}$$

where the extra parameter c is defined by

$$c = \int_0^1 (u - u^3)dy. \tag{41}$$

The parameters σ and c are related by $\sigma = c + \int_0^1 u^3 dy$. Therefore, if one varies c and solves for (40), then the parameter σ is uniquely determined.

Remark 5.1. *There exists a branch of constant solutions $(c, u(c))$ of (40) such that $u(c) - u(c)^3 = c$. For $c^* \stackrel{\text{def}}{=} \sqrt{1/3} - (\sqrt{1/3})^3$, the branch undergoes a saddle-node bifurcation at the parameter values $c = -c^*$ and $c = c^*$. We refer to the left picture in Figure 5 for a geometric interpretation. A bifurcation curve from the constant solution $u = u(c)$ is given by $\delta(\lambda, c) \stackrel{\text{def}}{=} 1 - 4\pi^2/\lambda - 3u(c)^2 = 0$. Hence, one can investigate the manifold of equilibria in the region $\mathcal{R} \stackrel{\text{def}}{=} \{(\lambda, c) \mid \delta(\lambda, c) > 0\}$ which is above the curve $\delta(\lambda, c) = 0$ in the (λ, c) plane, see Figure 5.*

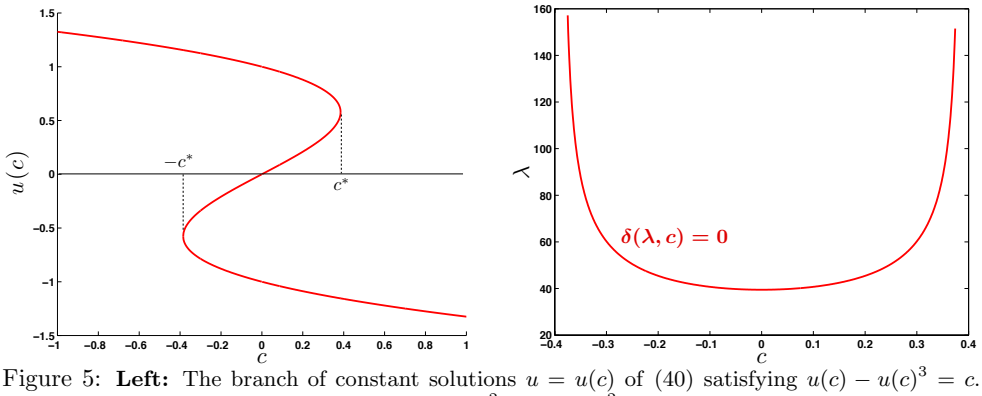

Figure 5: **Left:** The branch of constant solutions $u = u(c)$ of (40) satisfying $u(c) - u(c)^3 = c$. **Right:** The bifurcation curve $\delta(\lambda, c) = 1 - 4\pi^2/\lambda - 3u(c)^2 = 0$ associated to the piece of the solution curve $\{(c, u(c)) \mid -c^* < c < c^* \text{ and } u(-c^*) < u < u(c^*)\}$.

We expand solutions of (40) in the Fourier basis $\{\cos(k\pi y) \mid k = 0, 1, 2, \ldots\}$ as follows:

$$u(y) = a_0 + 2\sum_{k=1}^{\infty} a_k \cos(k\pi y).$$

Define $a = (a_k)_{k \geq 0}$ to be the infinite dimensional vector of Fourier coefficients of the expansion of u, $p \stackrel{\text{def}}{=} (\lambda, c)$ and let $x \stackrel{\text{def}}{=} (p, a)$. So (40) takes the form

$$f_k(x) \stackrel{\text{def}}{=} \mu_k(\lambda) a_k - (a^3)_k - \delta_{k,0} c = 0, \quad k \geq 0 \tag{42}$$

where $\mu_k(\lambda) = 1 - \pi^2 k^2/\lambda$ are the eigenvalues of the linear operator in (40), where $\delta_{k,l}$ is the Kronecker symbol and where we used the notation

$$(a * b * c)_k = \sum_{\substack{k_1+k_2+k_3=k \\ k_j \in \mathbb{Z}}} a_{|k_1|} b_{|k_2|} c_{|k_3|}, \quad a^3 = a * a * a.$$

From (42), we define $f = (f_k)_{k\geq 0}$. It can be shown that looking for solutions of (40) is equivalent to looking for solutions of $f(x) = 0$ in the Banach space $X = \mathbb{R}^2 \times \Omega^q$, where $\Omega^q = \{a = (a_k)_{k\geq 0} : \|a\|_q < \infty\}$ is the Banach space of infinite sequences algebraically decaying to 0 at least as fast as k^{-q} with *decay rate* $q > 1$ (e.g. see [13]). The regularity estimates given by Lemma A.4 in Appendix A can be used to show that if $a \in \Omega^q$, then $a^3 \in \Omega^q$. Since $\mu_k(\lambda) = 1 - \pi^2 k^2/\lambda$, one concludes that f given component-wise by (42) is defined as $f : \mathbb{R}^2 \times \Omega^q \to \Omega^{q-2}$. Consider the finite dimensional reduction $f^{(m)} : \mathbb{R}^{m+2} \to \mathbb{R}^m$ of f defined in (42) by $f^{(m)}(x_F) = (f_k(x_F, 0_\infty))_{k=0}^{m-1} \in \mathbb{R}^m$, where $x_F = (\lambda, c, a_0, a_1, \ldots, a_{m-1}) \in \mathbb{R}^{m+2}$. Assume that one has computed $\bar{x}_0, \bar{x}_1, \bar{x}_2 \in \mathbb{R}^{m+2}$ such that $f^{(m)}(\bar{x}_i) \approx 0$ for each $i = 0, 1, 2$ and that $\dim\left(\ker\left(Df^{(m)}(\bar{x}_i)\right)\right) = 2$. For each $i = 1, 2, 3$, define $\bar{\Phi}_i = [\phi_1^i \ \phi_2^i]$ the $(m+2) \times 2$ matrix whose columns are given by two linearly independent mutually orthonormal vectors spanning $\ker\left(Df^{(m)}(\bar{x}_i)\right)$. Moreover, assume that the frames $\bar{\Phi}_i$ have been "rotated" as described in Section 3.1.3.

As in Section 2, let $\bar{x}_s = \bar{x}_0 + s_1(\bar{x}_1 - \bar{x}_0) + s_2(\bar{x}_2 - \bar{x}_0)$ and $\bar{\Phi}_s = \bar{\Phi}_0 + s_1(\bar{\Phi}_1 - \bar{\Phi}_0) + s_2(\bar{\Phi}_2 - \bar{\Phi}_0)$. Denote $\bar{x}_s = (\lambda_s, c_s, a_s)$ and $\bar{x}_i = (\bar{\lambda}_i, \bar{c}_i, \bar{a}_i)$. Define the Banach space $W = \mathbb{R}^2 \times \Omega^{q-2}$. Consider $\mathcal{F}_s : X \to W$ as in (8) and consider the finite dimensional reduction $\mathcal{F}_s^{(m)} : \mathbb{R}^{m+2} \to \mathbb{R}^{m+2}$ defined by

$$\mathcal{F}_s^{(m)}(x_F) \stackrel{\text{def}}{=} \begin{pmatrix} \bar{\Phi}_s^T(x_F - \bar{x}_s) \\ f^{(m)}(x_F) \end{pmatrix}.$$

As in Section 2, define the linear operator $A : W \to X$ as follows. Assume we computed an invertible matrix A_m such that $A_m \approx D\mathcal{F}_0^{(m)}(\bar{x}_0)^{-1}$ and define A as in (9), where the tail of A is given by $\mu_k^{-1} = (1 - \pi^2 k^2/\bar{\lambda}_0)^{-1}$, for $k \geq m$. Then, A maps W to X and one can define the Newton-like operator $T_s \colon X \to X$ given by $T_s(x) = x - A\mathcal{F}_s(x)$. As already mentioned in Section 2, the idea of the construction of the local charts is to define the radii polynomials introduced in Definition 2.4. Hence, we need to consider the bounds Y and Z satisfying (11) and (12), respectively. To compute $Y = (Y_k)_{k\geq -2}$ satisfying (11), we expand $f(\bar{x}_s)$ as a polynomial in the variables s_1 and s_2. Note that the components Y_{-2} and Y_{-1} correspond to the bounds associated to the first two components of $\mathcal{F}_s$. For each $i, j \geq 0$ such that $2 \leq i + j \leq 3$ and for each $k \geq 0$, consider $y_k^{(i,j)} = y_k^{(i,j)}(\bar{x}_0, \bar{x}_1, \bar{x}_2)$ such that

$$\begin{aligned} f_k(\bar{x}_s) &= \mu_k(\lambda_s)(a_s)_k - (a_s^3)_k - \delta_{k,0} c_s \\ &= f_k(\bar{x}_0) + s_1[f_x(\bar{x}_0)(\bar{x}_1 - \bar{x}_0)]_k + s_2[f_x(\bar{x}_0)(\bar{x}_2 - \bar{x}_0)]_k + \sum_{\substack{2\leq i+j\leq 3 \\ i,j\geq 0}} y_k^{(i,j)} s_1^i s_2^j, \end{aligned}$$

where

$$
\begin{aligned}
[f_x(\bar{x}_0)(\bar{x}_1-\bar{x}_0)]_k &= \left(1-\frac{\pi^2k^2}{\bar{\lambda}_0}\right)[\bar{a}_2-\bar{a}_0]_k \\
&\quad + \frac{\pi^2k^2}{\bar{\lambda}_0^2}(\bar{\lambda}_2-\bar{\lambda}_0)[\bar{a}_0]_k - 3[\bar{a}_0^2(\bar{a}_2-\bar{a}_0)]_k - \delta_{k,0}(\bar{c}_2-\bar{c}_0) \\
[f_x(\bar{x}_0)(\bar{x}_2-\bar{x}_0)]_k &= \left(1-\frac{\pi^2k^2}{\bar{\lambda}_0}\right)[\bar{a}_1-\bar{a}_0]_k \\
&\quad + \frac{\pi^2k^2}{\bar{\lambda}_0^2}(\bar{\lambda}_1-\bar{\lambda}_0)[\bar{a}_0]_k - 3[\bar{a}_0^2(\bar{a}_1-\bar{a}_0)]_k - \delta_{k,0}(\bar{c}_1-\bar{c}_0).
\end{aligned}
$$

The coefficients $y_k^{(i,j)}$ are given in Table 3 in Appendix B. Note that some of these coefficients depend on a $\xi \in [\bar{\lambda}_0,\ \lambda_s]$, with $\lambda_s = \bar{\lambda}_0 + s_1(\bar{\lambda}_1-\bar{\lambda}_0) + s_2(\bar{\lambda}_2-\bar{\lambda}_0)$, which comes from taking a Taylor expansion of the function $s=(s_1,s_2) \mapsto \mu_k(\lambda_s)$ around $s=(0,0)$. In practice, ξ is replaced by the interval $\bar{\lambda}_0 + [0,1](\bar{\lambda}_1-\bar{\lambda}_0) + [0,1](\bar{\lambda}_2-\bar{\lambda}_0)$ and $|y_k^{(i,j)}|$ is estimated with interval arithmetic. Note that all the discrete convolutions in Table 3 are finite sums that can be rigorously estimated combining interval arithmetic with the fast Fourier transform (FFT) algorithm (e.g. see [20]). We then obtain rigorous upper bounds $Y_k^{(i,j)}$ for the terms $|y_k^{(i,j)}|$. Using formula (20), we define $Y_F = (Y_{-2}, Y_{-1}, \dots, Y_{m-1})$.

Let us now choose the M from assumption **A1** that assumes Y_k can be taken to be 0 for all $k \geq M$. Since $(\bar{a}_0)_k = (\bar{a}_1)_k = (\bar{a}_2)_k = 0$ for $k \geq m$, then for every $k \geq 3m-2$, $f_k(\bar{x}_0) = [f_x(\bar{x}_0)(\bar{x}_1-\bar{x}_0)]_k = [f_x(\bar{x}_0)(\bar{x}_2-\bar{x}_0)]_k = 0$ and $y_k^{(i,j)} = 0$ for all i,j. Indeed, for vectors a,b,c satisfying $a_k = b_k = c_k = 0$ for $k \geq m$, $(a*b*c)_k = 0$ for $k \geq 3m-2$. Hence, letting $M = 3m-2$, we set $Y_k = 0$, for $k \geq M$. To define Y_k for $m \leq k \leq M-1$, consider $\mu_k = \mu_k(\bar{\lambda}_0) = 1-\pi^2k^2/\bar{\lambda}_0$ and use (21).

To ease the computation of the bound $Z = (Z_k)_{k\geq -2}$ satisfying (12), we consider the expansion (22), with the coefficients $z_k^{(\ell,i,j)}$ being given in Table 4 in Appendix B. Note that the components Z_{-2} and Z_{-1} correspond to the bounds associated to the first two components of $\mathcal{F}_s$.

Using the fact that for $s=(s_1,s_2) \in \Delta$, $|s_1|,|s_2| \leq 1$ and the fact that $|(\tilde{b}_1)_k|, |(\tilde{b}_1)_k| \leq \omega_k^{-q}$, consider the intermediate bounds $\hat{z}_k^{(\ell)} = \hat{z}_k^{(\ell)}(\bar{x}_0, \bar{x}_1, \bar{x}_2, \bar{\Phi}_0, \bar{\Phi}_1, \bar{\Phi}_2)$ such that

$$
\left| \sum_{i=0}^{(4-\ell)} \sum_{j=0}^{(4-\ell-i)} z_k^{(\ell,i,j)} s_1^i s_2^j \right| \leq \hat{z}_k^{(\ell)}. \tag{43}
$$

The coefficients $\hat{z}_k^{(\ell)}$ are given in Table 5 in Appendix B. Since many discrete convolutions in Table 5 are infinite, we use the following result to estimate them.

Lemma 5.2. *Consider a decay rate $q \geq 2$ and $a,b,c \in \Omega^q$, where Ω^q is defined in (4). Consider a computational parameter M and define $a^{(M)} = (a_0, a_1, \dots, a_{M-1}) \in \mathbb{R}^M$. Define $b^{(M)}$, $c^{(M)}$ similarly. Consider $\varepsilon_k^{(3)} = \varepsilon_k^{(3)}(q,M,M)$ as in (50). Then, for $k \in \{0,\dots,M-1\}$,*

$$
|(a*b*c)_k| \leq \left| \left(a^{(M)} * b^{(M)} * c^{(M)}\right)_k \right| + 3(\|a\|_q \|b\|_q \|c\|_q)\varepsilon_k^{(3)}.
$$

Proof. The result follows from Lemma A.6 in Appendix A. □

Using Lemma 5.2, we obtain rigorous upper bounds $Z_k^{(\ell)}$ for the terms $\hat{z}_k^{(\ell)}$ from Table 5. Using formula (24) and (25), we define Z_k for $k \in \{-2,-1,\dots,M-1\}$. Now, to obtain the *uniform* polynomial bound $\tilde{Z}_M(r)$ of assumption **A2**, we use the following.

Lemma 5.3. *Consider a decay rate $q \geq 2$ and $a, b, c \in \Omega^q$, where Ω^q is defined in (4). Consider $\alpha_k^{(3)}$ as defined in (49). Then, for any $k \geq M \geq 6$, $\alpha_k^{(3)} \leq \alpha_M^{(3)}$ and*

$$|(a * b * c)_k| \leq (\|a\|_q \|b\|_q \|c\|_q) \frac{\alpha_M^{(3)}}{\omega_k^q}. \tag{44}$$

Proof. The result follows from Lemma A.4 and Lemma A.5. □

Lemma 5.4. *Consider $\lambda_0 > 0$ and a number M such that*

$$M > \frac{\sqrt{\lambda_0}}{\pi}. \tag{45}$$

Then, for every $k \geq M$, one has that $\frac{1}{|\mu_k(\lambda_0)|} \leq \frac{\lambda_0}{\pi^2 M^2 - \lambda_0}$ and that $\left|\frac{\pi^2 k^2}{\mu_k(\lambda_0)}\right| \leq \frac{\pi^2 M^2 \lambda_0}{\pi^2 M^2 - \lambda_0}$.

Proof. Considering $k \geq M$, one has that $|\mu_k(\lambda_0)| = |1 - \frac{1}{\lambda_0} k^2 \pi^2| = \frac{1}{\lambda_0} k^2 \pi^2 - 1 = \frac{k^2 \pi^2 - \lambda_0}{\lambda_0} \geq \frac{\pi^2 M^2 - \lambda_0}{\lambda_0} > 0$. That implies that $\frac{1}{|\mu_k(\lambda_0)|} \leq \frac{\lambda_0}{\pi^2 M^2 - \lambda_0}$. Also, $\left|\frac{\pi^2 k^2}{\mu_k(\lambda_0)}\right| = \frac{\pi^2 k^2 \lambda_0}{k^2 \pi^2 - \lambda_0} \leq \frac{\pi^2 M^2 \lambda_0}{\pi^2 M^2 - \lambda_0}$, since the function $x \mapsto \frac{\pi^2 x^2}{\pi^2 x^2 - \lambda_0}$ decreases for $x \geq M$. □

Using the results of Lemma 5.3 and Lemma 5.4, we introduce the asymptotic polynomial bound $\tilde{Z}_M(r)$ satisfying (16). For $\ell = 1, 2, 3$, consider the asymptotic bound $\tilde{Z}_M^{(\ell)}$ such that for $k \geq M$ and for all $s \in D$,

$$\sup_{b_1, b_2 \in B(r)} \left| [DT_s(\bar{x}_s + b_1) b_2]_k \right| \leq \sum_{\ell=1}^{3} \frac{1}{|\mu_k(\lambda_0)|} \hat{z}_k^{(\ell)} r^\ell \leq \left(\sum_{\ell=1}^{3} \tilde{Z}_M^{(\ell)} r^\ell \right) \frac{1}{\omega_k^q}, \tag{46}$$

where the $\tilde{Z}_M^{(\ell)}$ can be found in Table 6 in Appendix B. Using (46) and the coefficients of Table 6, define the tail radii polynomial (18). Again, note that some of the coefficients in Table 6 depend on a ξ between $\bar{\lambda}_0$ and $\lambda_s = \bar{\lambda}_0 + s_1(\bar{\lambda}_1 - \bar{\lambda}_0) + s_2(\bar{\lambda}_2 - \bar{\lambda}_0)$ which comes from taking a Taylor expansion of the function $s = (s_1, s_2) \mapsto \mu_k(\lambda_s)$ around $s = (0, 0)$. In practice, ξ is replaced by the interval $\bar{\lambda}_0 + [0, 1](\bar{\lambda}_1 - \bar{\lambda}_0) + [0, 1](\bar{\lambda}_2 - \bar{\lambda}_0)$ and $\tilde{Z}_M^{(\ell)}$ is finally obtained with interval arithmetic.

We have finally all the ingredients to construct the radii polynomials $\{p_k(r)\}_{k=-2}^{M}$ of Definition 2.4 with interval arithmetic. Once this is done, we can verify (if possible) the hypotheses of Lemma 2.5 and then the smoothness hypothesis (31). As mentioned above, this procedure is referred to as the *verification* of a simplex. Therefore, our algorithm provides precise bounds in the Banach space around each approximate simplex within which a genuine smooth local chart of the manifold is guaranteed to exist in the mathematically rigorous sense. Using the method of Section 3 to obtain a triangulation of the manifold based on successes or failures of the verification of each simplex, we can conclude, using the theory of Section 4, that we performed a rigorous computation of the smooth C^ℓ manifold. We now present some results.

Example 5.5. As a first example, we computed a manifold of equilibria of (39) identified by the following constraints:

$$\lambda \in [39, 41], \ \delta(\lambda, c) \geq 10^{-3}.$$

For the projection $f^{(m)}$, we took $m = 40$, i.e., we kept the first 40 Fourier modes of solutions u of (39). We also fixed the algebraic decay rate of the Banach space Ω^q as defined

in (4) to be $q = 2$. We started the computation from a point $x_0 \in \mathbb{R}^{42}$ numerically on the manifold. We obtained x_0 by fixing $c = 0$ and following in λ (via a standard path-following algorithm) the branch of equilibria that bifurcates from the trivial solution at $\lambda = 4\pi^2$, up to $\lambda \approx 40$. The actual coordinates of x_0 can be downloaded from [24]. Furthermore, we chose $h_0 = 4.5 \times 10^{-3}$ and $h_{\min} = 10^{-5}$, see Section 3 for the meaning of these parameters.

Starting from x_0, we applied the method described in Section 3, with the (unsubstantial) exception reported in a Remark below. The computation was completed successfully (i.e. it terminated due to absence of frontal nodes) and resulted in a database made of 57960 nodes and 114059 simplices. The number of rejected steps (due to verification failures) was 21585, which accounts for nearly 16% of the total work. At the end, all simplices had been successfully verified, with 6814 simplices requiring 1 splitting and 13 simplices requiring 2 to 5 splittings.

Denote by $\mathcal{S}_1$ the simplicial approximation obtained as described above. A geometric representation of $\mathcal{S}_1$ is presented in Figure 6. On each simplex $\sigma \in \mathcal{S}_1$ the hypotheses of Lemmas 2.5 and 2.6 were verified yielding a map $\tilde{x}_\sigma \colon \Delta \to X$ such that $\mathcal{F}_s(\tilde{x}_\sigma(s)) = 0$. By Lemma 2.6 there is an $\varepsilon = \varepsilon(\sigma) > 0$ such that $\tilde{x}_\sigma$ can be extended to a C^ℓ diffeomorphism, also denoted by $\tilde{x}_\sigma$, on $\Delta_\varepsilon = \{s = (s_1, s_2) \mid s_1, s_2 \geq -\varepsilon \text{ and } s_1 + s_2 \leq 1 + \varepsilon\}$. For each $\sigma \in \mathcal{S}_1$, let $U_\sigma = \tilde{x}_\sigma(\Delta_\varepsilon)$.

Theorem 5.6. *Consider $\mathcal{S}_1$, the simplicial approximation defined above. Then, the set*

$$\mathcal{M}_1 \stackrel{\text{def}}{=} \bigcup_{\sigma \in \mathcal{S}_1} U_\sigma$$

is a smooth two-dimensional manifold implicitly defined by the infinite dimensional nonlinear equation $f = 0$, with f given component-wise by (42)*. Moreover, $\mathcal{M}_1$ yields a smooth two-dimensional manifold of equilbria of the Cahn-Hilliard equation* (39)*. Furthermore, for each $\sigma \in \mathcal{S}_1$ defined by $\sigma = \{\bar{x}_s \mid s \in \Delta\}$, one has that*

$$\sup_{s \in \Delta} \|\tilde{x}_\sigma(s) - \bar{x}_s\|_X \leq r,$$

where $r = r(\sigma)$ is the radius obtained by solving the radii polynomials as in Lemma 2.5.

Example 5.7. As a second example, we computed again a manifold of equilibria of the Cahn-Hilliard equation, this time identified by the constraints:

$$\lambda \in [69.9, 70.1], \ \delta(\lambda, c) \geq 0.2\,.$$

As in Example 5.5, we kept $m = 40$ Fourier modes, and chose the decay rate for Ω^q to be $q = 2$. We started the computation from a point $x_0 \in \mathbb{R}^{42}$ numerically on the manifold, obtained just like in Example 5.5, but with $\lambda \approx 70$ (again, see [24] for the actual coordinates of x_0), and chose $h_0 = 10^{-2}$ and $h_{\min} = 10^{-5}$. Also in this case, the computation terminated successfully, this time with a resulting database of 24168 nodes and 47658 simplices. Rejected steps were 7646, i.e., nearly 14% of the total work. All simplices were successfully verified, with 3446 of them requiring 1 splitting.

Denote by $\mathcal{S}_2$ the simplicial approximation obtained as described above. $\mathcal{S}_2$ is depicted in Figure 7. On each simplex $\sigma \in \mathcal{S}_2$ the hypotheses of Lemmas 2.5 and 2.6 were verified yielding a map $\tilde{x}_\sigma \colon \Delta \to X$ such that $\mathcal{F}_s(\tilde{x}_\sigma(s)) = 0$. By Lemma 2.6, there is an $\varepsilon = \varepsilon(\sigma) > 0$ such that $\tilde{x}_\sigma$ can be extended to a C^ℓ diffeomorphism, also denoted by $\tilde{x}_\sigma$, on Δ_ε. For each $\sigma \in \mathcal{S}_2$, let $U_\sigma = \tilde{x}_\sigma(\Delta_\varepsilon)$.

Theorem 5.8. *Consider $\mathcal{S}_2$ the simplicial approximation defined above. Then, the set*

$$\mathcal{M}_2 \stackrel{\text{def}}{=} \bigcup_{\sigma \in \mathcal{S}_2} U_\sigma$$

is a smooth two-dimensional manifold implicitly defined by the infinite dimensional nonlinear equation $f = 0$, with f given component-wise by (42). Moreover, $\mathcal{M}_2$ yields a smooth two-dimensional manifold of equilbria of the Cahn-Hilliard equation (39). Furthermore, for each $\sigma \in \mathcal{S}_2$ defined by $\sigma = \{\bar{x}_s \mid s \in \Delta\}$, one has that

$$\sup_{s \in \Delta} \|\tilde{x}_\sigma(s) - \bar{x}_s\|_X \leq r,$$

where $r = r(\sigma)$ is the radius obtained by solving the radii polynomials as in Lemma 2.5.

Remark 5.9. The only exception to the strategy described in Section 3 is that, during the numerical triangulation of the manifold, verification of simplices was (temporarily) performed –without– interval arithmetic. This is because the overhead associated to the use of interval arithmetic makes the computation impossible to be performed on a single computing unit. Hence, proper verification of simplices was postponed to a distributed computed environment, where it was spread over 500 processors. To witness the benefit of this strategy, verification of all simplices for the computation outlined in Example 5.5 required 39 hours (the duration of the longest-lasting process), with a total CPU time of approximately 680 days, while that of Example 5.7 required 18 hours, and a total CPU time of approximately 206 days, whereas building the databases for the two triangulations required, respectively, approximately 12 and 4 hours on a single processing unit.

Remark 5.10. The software was developed in MATLAB, and interval arithmetics computations were carried out by the toolbox INTLAB [21]. The construction of the database for the triangulations was performed on a desktop computer equipped with Intel Core 2 Duo E6400 2.13GHz CPU and 2 GB of RAM, while verification of the simplices was performed on the *PACE HPC environment* at the Georgia Institute of Technology. The complete database of nodes and simplices for both computation above, as well as the MATLAB code used to run the verification, can be found at [24].

Remark 5.11. The computation times reported in Remark 5.9 are admittedly long, and ought to be explained. On the one hand, as we already pointed out in Section 3, the construction of the triangulation is slowed down by the verification process, which, even if performed without the use of interval arithmetic, greatly penalizes the step-length and, consequently, the computational effort needed to cover a given portion of a manifold. If the continuation was to be performed without verification, it would be completed at a fraction of the cost (based on our experience, we expect this "fraction" to be below 1/100). On the other hand, the verification of simplices with interval arithmetic, which we postponed to a distributed computing environment, is currently implemented under INTLAB/MATLAB, which is not an environment optimized for performance. The verification stage would greatly benefit of being implemented in a better performing language, and this is an aspect that we plan to tackle in the future.

6 Conclusion

In this paper we introduce a new rigorous multi-parameter continuation method to compute smooth two-dimensional manifolds implicitly defined by zeros of nonlinear operators defined

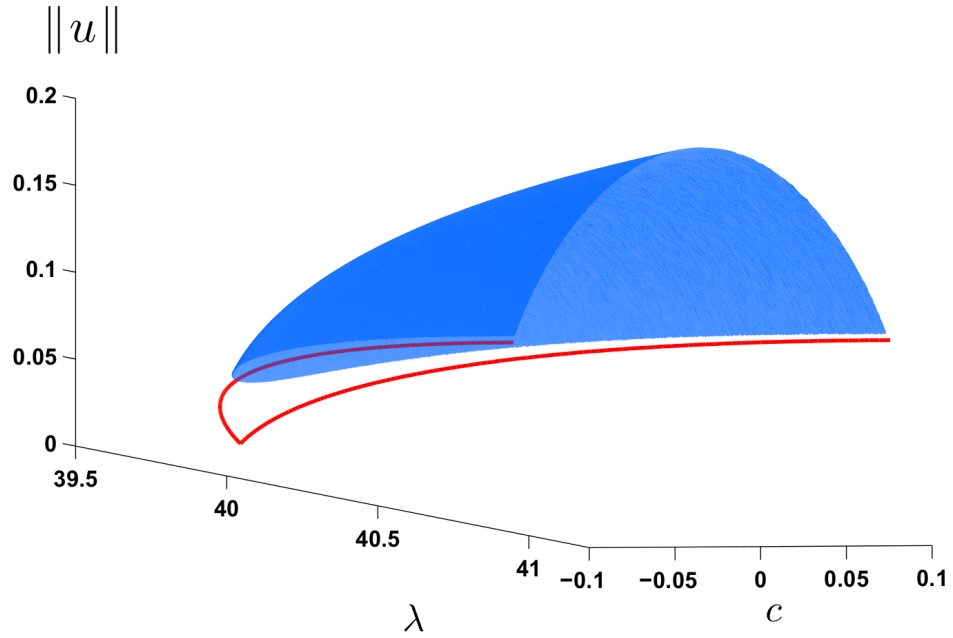

Figure 6: The solution manifold of Theorem 5.6. On this plot, the L^2 norm of the solution u is depicted. The red curve corresponds to the curve of constant equilibria of the 1D Cahn-Hilliard equation (39) from which the solution manifold bifurcates. The curve of constant solutions together with its corresponding (λ, c) parameter values can be found in Figure 5.

on infinite dimensional Banach spaces. The method is applied to compute two portions of a two-dimensional manifold of equilibria of the 1D Cahn-Hilliard PDE.

The method proved itself robust and successful when applied to the 1D Cahn-Hilliard equation. Yet, of course, we believe there is room for improvement. Rigorously computing large portions of a manifold can be burdensome. This is mostly due to the high computational cost involved in verifying a simplex with interval arithmetic. This is a motivation to try to minimize the number of simplices needed to "cover" a given portion of a manifold, as well as the number of simplices rejected due to verification failure. This is work in progress. Another improvement concerns the correct handling of situations where overlap of frontal simplices of the triangulation is detected. This also is work in progress. Note that we did not detect any overlap in the Examples presented in Section 5. We now conclude the paper by discussing future directions.

We believe it would interesting to explore the possibility of rigorously detecting bifurcations, for instance those related to loss of rank of the Jacobian matrix. The smooth singular value decomposition would be a useful tool for this project, see [22]. It would also be valuable to try to prove existence of cusp bifurcations in the two dimensional manifold of equilibria of the 2D Cahn-Hilliard model as numerically suggested in [4]. Another interesting problem would be to extend the work of [23] and compute two-dimensional manifolds of connecting

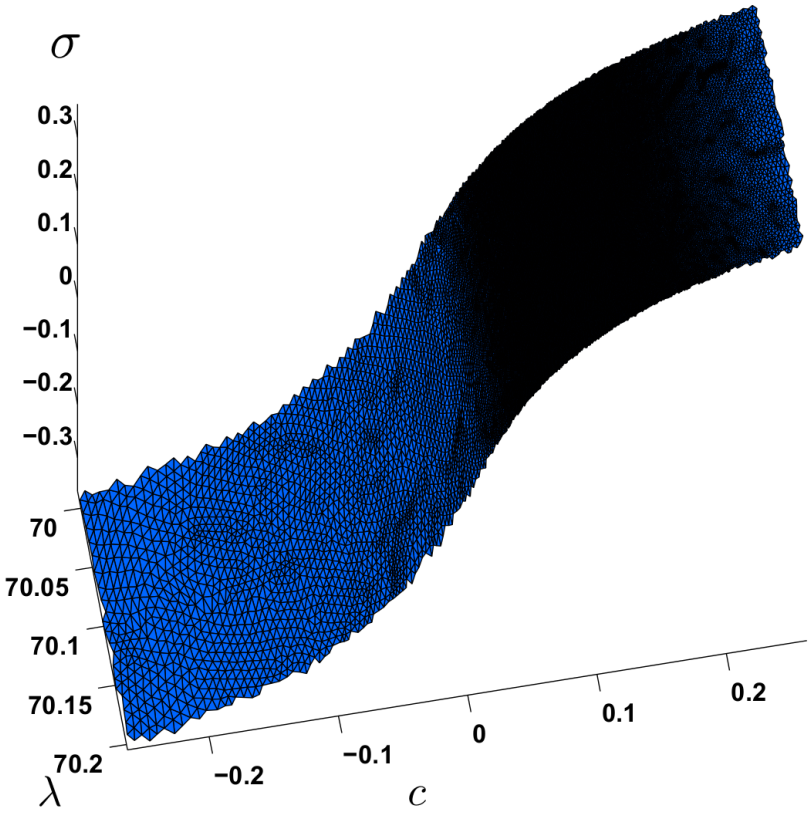

Figure 7: The solution manifold of Theorem 5.8. On this plot, the total mass σ of the solution u is depicted.

orbits in the Gray-Scott model for autocatalytic reaction.

Acknowledgments

The authors would like to thank the anonymous referees for helpful comments and suggestions. Part of this work was done while the third author was visiting the School of Mathematics of the Georgia Institute of Technology, whose hospitality and support is gratefully acknowledged.

A Convolution estimates

In this Appendix, we provide the necessary convolution estimates required to construct the radii polynomials for the Cahn-Hilliard equation studied in Section 5. We decided to

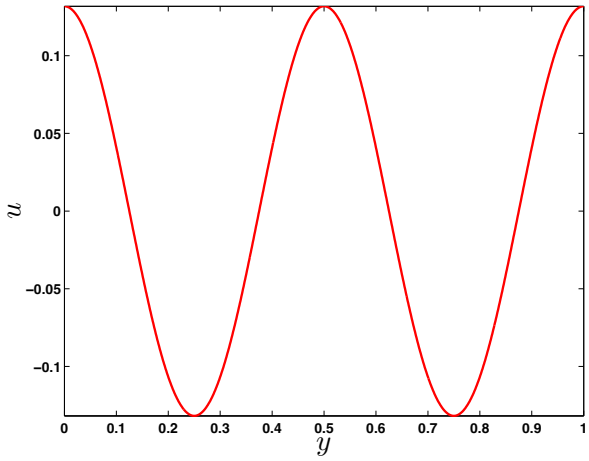

Figure 8: Profile of the solution $u(y)$ corresponding to the initial point $x_0 \in \mathbb{R}^{42}$ numerically on the manifold (the actual coordinates of x_0 can be downloaded from [24]). This point correspond to one of the equilibrium solution on the manifold of Theorem 5.6 at $(\lambda, c) = (40, 0)$.

include all formulas and proofs so that the paper is self-contained. Note, however, that these analytic convolution estimates are taken directly from [15] for estimates concerning quadratic and cubic nonlinearities.

Consider a decay rate $q \geq 2$, a computational parameter $M \geq 6$ and define, for $k \geq 3$,

$$\gamma_k = \gamma_k(q) \stackrel{\text{def}}{=} 2\left[\frac{k}{k-1}\right]^q + \left[\frac{4\ln(k-2)}{k} + \frac{\pi^2-6}{3}\right]\left[\frac{2}{k}+\frac{1}{2}\right]^{q-2}. \tag{47}$$

Lemma A.1. *For $q \geq 2$ and $k \geq 4$ we have*

$$\sum_{k_1=1}^{k-1} \frac{k^q}{k_1^q (k-k_1)^q} \leq \gamma_k.$$

Proof. First observe that

$$\begin{aligned}
\sum_{k_1=1}^{k-1} \frac{k^q}{k_1^q (k-k_1)^q} &= 2\left[\frac{k}{k-1}\right]^q + k^{q-1} \sum_{k_1=2}^{k-2} \frac{k}{k_1^q (k-k_1)^q} \\
&= 2\left[\frac{k}{k-1}\right]^q + k^{q-1}\left[\sum_{k_1=2}^{k-2} \frac{k-k_1}{k_1^q (k-k_1)^q} + \sum_{k_1=2}^{k-2} \frac{k_1}{k_1^q (k-k_1)^q}\right] \\
&= 2\left[\frac{k}{k-1}\right]^q + k^{q-1}\left[\sum_{k_1=2}^{k-2} \frac{1}{k_1^q (k-k_1)^{q-1}} + \sum_{k_1=2}^{k-2} \frac{1}{k_1^{q-1} (k-k_1)^q}\right] \\
&= 2\left[\frac{k}{k-1}\right]^q + 2\sum_{k_1=2}^{k-2} \frac{k^{q-1}}{k_1^{q-1} (k-k_1)^q}.
\end{aligned}$$

Using the above we define

$$\phi_k^{(q)} := \sum_{k_1=2}^{k-2} \frac{k^{q-1}}{k_1^{q-1}(k-k_1)^q} = \frac{1}{2}\sum_{k_1=2}^{k-2} \frac{k^q}{k_1^q(k-k_1)^q}.$$

We then obtain the following recurrence inequality

$$\begin{aligned}
\phi_k^{(q)} &= \sum_{k_1=2}^{k-2} \frac{k^{q-1}}{k_1^{q-1}(k-k_1)^q} = k^{q-2}\sum_{k_1=2}^{k-2} \frac{(k-k_1)+k_1}{k_1^{q-1}(k-k_1)^q} \\
&= \frac{1}{k}\sum_{k_1=2}^{k-2} \frac{k^{q-1}}{k_1^{q-1}(k-k_1)^{q-1}} + \sum_{k_1=2}^{k-2} \frac{k^{q-2}}{k_1^{q-2}(k-k_1)^q} \\
&\leq \frac{1}{k}\sum_{k_1=2}^{k-2} \frac{k^{q-1}}{k_1^{q-1}(k-k_1)^{q-1}} + \frac{1}{2}\sum_{k_1=2}^{k-2} \frac{k^{q-2}}{k_1^{q-2}(k-k_1)^{q-1}} \quad = \quad \left[\frac{2}{k}+\frac{1}{2}\right]\phi_k^{(q-1)}.
\end{aligned}$$

Applying the above inequality $q-2$ times we get

$$\phi_k^{(q)} \leq \phi_k^{(2)}\left[\frac{2}{k}+\frac{1}{2}\right]^{q-2}.$$

Also

$$\begin{aligned}
\phi_k^{(2)} &= \sum_{k_1=2}^{k-2} \frac{k}{k_1(k-k_1)^2} = \sum_{k_1=2}^{k-2} \frac{1}{k_1(k-k_1)} + \sum_{k_1=2}^{k-2} \frac{1}{(k-k_1)^2} \\
&= \frac{1}{k}\left[\sum_{k_1=2}^{k-2} \frac{1}{k_1} + \sum_{k_1=2}^{k-2} \frac{1}{k-k_1}\right] + \sum_{k_1=2}^{k-2} \frac{1}{(k-k_1)^2} \\
&= \frac{2}{k}\sum_{k_1=2}^{k-2} \frac{1}{k_1} + \sum_{k_1=2}^{k-2} \frac{1}{k_1^2} \leq \frac{2}{k}\ln(k-2) + \frac{\pi^2}{6} - 1.
\end{aligned}$$

Using the above inequalities we get

$$\begin{aligned}
\sum_{k_1=1}^{k-1} \frac{k^q}{k_1^q(k-k_1)^q} &= 2\left[\frac{k}{k-1}\right]^q + 2\phi_k^{(q)} \leq 2\left[\frac{k}{k-1}\right]^q + 2\phi_k^{(2)}\left[\frac{2}{k}+\frac{1}{2}\right]^{q-2} \\
&\leq 2\left[\frac{k}{k-1}\right]^q + \left[\frac{4\ln(k-2)}{k} + \frac{\pi^2-6}{3}\right]\left[\frac{2}{k}+\frac{1}{2}\right]^{q-2} \quad = \quad \gamma_k. \quad \square
\end{aligned}$$

Define the weights by

$$\omega_k^q := \begin{cases} 1, & \text{if } k=0 \\ |k|^q, & \text{if } k \neq 0. \end{cases}$$

Lemma A.2 (Quadratic estimates)**.** *Given a decay rate $q \geq 2$ and $M \geq 6$. For $k \in \mathbb{Z}$,*

define the quadratic asymptotic estimates $\alpha_k^{(2)} = \alpha_k^{(2)}(q, M)$ *by*

$$\alpha_k^{(2)} \stackrel{\text{def}}{=} \begin{cases} 1 + 2\sum_{k_1=1}^{M} \frac{1}{\omega_{k_1}^{2q}} + \frac{2}{M^{2q-1}(2q-1)}, & \text{for } k = 0 \\ \sum_{k_1=1}^{M} \frac{2\omega_k^q}{\omega_{k_1}^q \omega_{k+k_1}^q} + \frac{2\omega_k^q}{(k+M+1)^q M^{q-1}(q-1)} & \\ \qquad +2 + \sum_{k_1=1}^{k-1} \frac{\omega_k^q}{\omega_{k_1}^q \omega_{k-k_1}^q}, & \text{for } 1 \le k \le M-1 \\ 2 + 2\sum_{k_1=1}^{M} \frac{1}{\omega_{k_1}^q} + \frac{2}{M^{q-1}(q-1)} + \gamma_M, & \text{for } k \ge M, \end{cases} \tag{48}$$

and for $k < 0$,

$$\alpha_k^{(2)} \stackrel{\text{def}}{=} \alpha_{|k|}^{(2)}.$$

Then, for any $k \in \mathbb{Z}$,

$$\sum_{\substack{k_1+k_2=k \\ k_j \in \mathbb{Z}}} \frac{1}{\omega_{k_1}^q \omega_{k_2}^q} \le \frac{\alpha_k^{(2)}}{\omega_k^q}.$$

Proof. For $k = 0$,

$$\begin{aligned} \sum_{\substack{k_1+k_2=0 \\ k_j \in \mathbb{Z}}} \frac{1}{\omega_{k_1}^q \omega_{k_2}^q} &= 1 + 2\sum_{k_1=1}^{M} \frac{1}{\omega_{k_1}^{2q}} + 2\sum_{k_1=M+1}^{\infty} \frac{1}{\omega_{k_1}^{2q}} \le 1 + 2\sum_{k_1=1}^{M} \frac{1}{\omega_{k_1}^{2q}} + \int_M^\infty \frac{dx}{x^{2q}} \\ &\le 1 + 2\sum_{k_1=1}^{M} \frac{1}{\omega_{k_1}^{2q}} + \frac{2}{M^{2q-1}(2q-1)} = \frac{\alpha_0^{(2)}}{\omega_0^q}. \end{aligned}$$

For $1 \le k \le M-1$, and recalling that the one-dimensional weights (2),

$$\begin{aligned} \sum_{\substack{k_1+k_2=k \\ k_j \in \mathbb{Z}}} \frac{1}{\omega_{k_1}^q \omega_{k_2}^q} &= \frac{1}{\omega_k^q}\left[\sum_{k_1=1}^{M} \frac{2\omega_k^q}{\omega_{k_1}^q \omega_{k+k_1}^q} + \sum_{k_1=M+1}^{\infty} \frac{2\omega_k^q}{\omega_{k_1}^q \omega_{k+k_1}^q} + \frac{2}{\omega_0^q} + \sum_{k_1=1}^{k-1} \frac{\omega_k^q}{\omega_{k_1}^q \omega_{k-k_1}^q}\right] \\ &\le \frac{1}{\omega_k^q}\left[\sum_{k_1=1}^{M} \frac{2\omega_k^q}{\omega_{k_1}^q \omega_{k+k_1}^q} + \frac{2\omega_k^q}{(k+M+1)^q}\int_M^\infty \frac{dx}{x^q} + 2 + \sum_{k_1=1}^{k-1} \frac{\omega_k^q}{\omega_{k_1}^q \omega_{k-k_1}^q}\right] \\ &\le \frac{1}{\omega_k^q}\left[\sum_{k_1=1}^{M} \frac{2\omega_k^q}{\omega_{k_1}^q \omega_{k+k_1}^q} + \frac{2\omega_k^q}{(k+M+1)^q M^{q-1}(q-1)} + 2 + \sum_{k_1=1}^{k-1} \frac{\omega_k^q}{\omega_{k_1}^q \omega_{k-k_1}^q}\right] = \frac{\alpha_k^{(2)}}{\omega_k^q}. \end{aligned}$$

Finally, for $k \geq M$, one gets from Lemma A.1 that

$$\begin{aligned}
\sum_{\substack{k_1+k_2=k \\ k_j \in \mathbb{Z}}} \frac{1}{\omega_{k_1}^q \omega_{k_2}^q} &= \frac{1}{\omega_k^q}\left[2\sum_{k_1=1}^{\infty} \frac{\omega_k^q}{\omega_{k_1}^q \omega_{k+k_1}^q} + \frac{2}{\omega_0^q} + \sum_{k_1=1}^{k-1} \frac{\omega_k^q}{\omega_{k_1}^q \omega_{k-k_1}^q}\right] \\
&\leq \frac{1}{\omega_k^q}\left[2\sum_{k_1=1}^{M} \frac{1}{\omega_{k_1}^q} + 2\sum_{k_1=M+1}^{\infty} \frac{1}{\omega_{k_1}^q} + \frac{2}{\omega_0^q} + \gamma_k\right] \\
&\leq \frac{1}{\omega_k^q}\left[2\sum_{k_1=1}^{M} \frac{1}{\omega_{k_1}^q} + 2\int_M^{\infty} \frac{dx}{x^q} + \frac{2}{\omega_0^q} + \gamma_M\right] \\
&\leq \frac{1}{\omega_k^q}\left[\sum_{k_1=1}^{M} \frac{2}{\omega_{k_1}^q} + \frac{2}{M^{q-1}(q-1)} + 2 + \gamma_M\right] = \frac{\alpha_k^{(2)}}{\omega_k^q}. \quad \square
\end{aligned}$$

Lemma A.3. *For any $k \in \mathbb{Z}$ with $|k| \geq M \geq 6$, we have that $\alpha_k^{(2)} \leq \alpha_M^{(2)}$.*

Proof. For $k \geq 6$, the fact that $\frac{\ln(k-1)}{k+1} \leq \frac{\ln(k-2)}{k}$ implies that $\gamma_{k+1}(q) \leq \gamma_k(q)$. By definition of $\alpha_k^{(2)}$, for $|k| \geq M$, one gets that $\alpha_k^{(2)} \leq \alpha_M^{(2)}$. $\square$

Lemma A.4 (Cubic estimates)**.** *Given $q \geq 2$ and $M \geq 6$. Let*

$$\Sigma_a^* := \sum_{k_1=1}^{M-1} \frac{\alpha_{k_1}^{(2)} M^q}{\omega_{k_1}^q (M-k_1)^q} + \alpha_M^{(2)}\left(\gamma_M - \sum_{k_1=1}^{M-1} \frac{1}{\omega_{k_1}^q}\right),$$

$\tilde{\alpha}_M^{(2)} := \max\left\{\alpha_k^{(2)} \mid k = 0, \ldots, M\right\}$, $\Sigma_b^* := \tilde{\alpha}_M^{(2)} \gamma_M$ *and* $\Sigma^* := \min\{\Sigma_a^*, \Sigma_b^*\}$. *Define the cubic asymptotic estimates $\alpha_k^{(3)} = \alpha_k^{(3)}(s, M)$ by*

$$\alpha_k^{(3)} \stackrel{\text{def}}{=} \begin{cases}
\alpha_0^{(2)} + 2\sum_{k_1=1}^{M-1} \frac{\alpha_{k_1}^{(2)}}{\omega_{k_1}^{2q}} + \frac{2\alpha_M^{(2)}}{(M-1)^{2q-1}(2q-1)}, & \text{for } k = 0 \\
\sum_{k_1=1}^{M-k} \frac{\alpha_{k+k_1}^{(2)} \omega_k^q}{\omega_{k_1}^q \omega_{k+k_1}^q} + \frac{\alpha_M^{(2)} \omega_k^q}{(M+1)^q (M-k)^{q-1}(q-1)} + \sum_{k_1=1}^{k-1} \frac{\alpha_{k_1}^{(2)} \omega_k^q}{\omega_{k_1}^q \omega_{k-k_1}^q} & \\
\quad + \sum_{k_1=1}^{M} \frac{\alpha_{k_1}^{(2)} \omega_k^q}{\omega_{k_1}^q \omega_{k+k_1}^q} + \frac{\alpha_M^{(2)} \omega_k^q}{(M+k+1)^q M^{q-1}(q-1)} + \alpha_k^{(2)} + \alpha_0^{(2)}, & \\
\qquad\qquad \text{for } 1 \leq k \leq M-1 & \\
\alpha_M^{(2)} \sum_{k_1=1}^{M} \frac{1}{\omega_{k_1}^q} + \frac{2\alpha_M^{(2)}}{M^{q-1}(q-1)} + \Sigma^* + \sum_{k_1=1}^{M} \frac{\alpha_{k_1}^{(2)}}{\omega_{k_1}^q} + \alpha_M^{(2)} + \alpha_0^{(2)}, & \text{for } k \geq M
\end{cases} \tag{49}$$

and for $k < 0$,

$$\alpha_k^{(3)} \stackrel{\text{def}}{=} \alpha_{|k|}^{(3)}.$$

Then, for any $k \in \mathbb{Z}$,

$$\sum_{\substack{k_1+k_2+k_3=k \\ k_j \in \mathbb{Z}}} \frac{1}{\omega_{k_1}^q \omega_{k_2}^q \omega_{k_3}^q} \leq \frac{\alpha_k^{(3)}}{\omega_k^q}.$$

Moreover, $\alpha_k^{(3)} \leq \alpha_M^{(3)}$, for all $k \geq M$.

Proof. In what follows, the estimates are obtained similarly as in the proof of Lemma A.2 with the difference that we often use the fact $\alpha_k^{(2)} \le \alpha_M^{(2)}$, for all $k \ge M$ (see e.g. Remark A.1 in [13]). For $k = 0$,

$$\sum_{\substack{k_1+k_2+k_3=0\\ k_j\in\mathbb{Z}}} \frac{1}{\omega_{k_1}^q \omega_{k_2}^q \omega_{k_3}^q} \quad \le \quad \alpha_0^{(2)} + 2\sum_{k_1=1}^{M-1} \frac{\alpha_{k_1}^{(2)}}{\omega_{k_1}^{2q}} + \frac{2\alpha_M^{(2)}}{(M-1)^{2q-1}(2q-1)} = \frac{\alpha_0^{(3)}}{\omega_0^q}.$$

For $k > 0$,

$$\begin{aligned}\sum_{\substack{k_1+k_2+k_3=k\\ k_j\in\mathbb{Z}}} \frac{1}{\omega_{k_1}^q \omega_{k_2}^q \omega_{k_3}^q} \quad \le \quad & \sum_{k_1=1}^{\infty} \left[\frac{1}{\omega_{k_1}^q} \frac{\alpha_{k+k_1}^{(2)}}{\omega_{k+k_1}^q}\right] + \sum_{k_1=1}^{k-1} \left[\frac{1}{\omega_{k_1}^q} \frac{\alpha_{k-k_1}^{(2)}}{\omega_{k-k_1}^q}\right] + \sum_{k_1=1}^{\infty} \left[\frac{1}{\omega_{k+k_1}^q} \frac{\alpha_{k_1}^{(2)}}{\omega_{k_1}^q}\right] \\ & + \frac{1}{\omega_0^q} \frac{\alpha_k^{(2)}}{\omega_k^q} + \frac{1}{\omega_k^q} \frac{\alpha_0^{(2)}}{\omega_0^q}.\end{aligned}$$

Consider $k \in \{1, \dots, M-1\}$. Since $\alpha_k^{(2)} \le \alpha_M^{(2)}$, for all $k \ge M$ by Lemma A.3, we have

$$\sum_{k_1=1}^{\infty} \frac{\alpha_{k+k_1}^{(2)}}{\omega_{k_1}^q \omega_{k+k_1}^q} \le \frac{1}{\omega_k^q} \left[\sum_{k_1=1}^{M-k} \frac{\alpha_{k+k_1}^{(2)} \omega_k^q}{\omega_{k_1}^q \omega_{k+k_1}^q} + \frac{\alpha_M^{(2)} \omega_k^q}{(M+1)^q (M-k)^{q-1}(q-1)}\right].$$

Similarly,

$$\sum_{k_1=1}^{\infty} \frac{\alpha_{k_1}^{(2)}}{\omega_{k_1}^q \omega_{k+k_1}^q} \le \frac{1}{\omega_k^q} \left[\sum_{k_1=1}^{M} \frac{\alpha_{k_1}^{(2)} \omega_k^q}{\omega_{k_1}^q \omega_{k+k_1}^q} + \frac{\alpha_M^{(2)} \omega_k^q}{(M+k+1)^q M^{q-1}(q-1)}\right].$$

From the definition of $\alpha_k^{(3)}$ for $k \in \{1, \dots, M-1\}$, one gets that

$$\sum_{\substack{k_1+k_2+k_3=k\\ k_j\in\mathbb{Z}}} \frac{1}{\omega_{k_1}^q \omega_{k_2}^q \omega_{k_3}^q} \le \frac{\alpha_k^{(3)}}{\omega_k^q}.$$

For $k \ge M$, using again that $\alpha_k^{(2)} \le \alpha_M^{(2)}$ by Lemma A.3, one gets that

$$\sum_{k_1=1}^{\infty} \frac{\alpha_{k+k_1}^{(2)}}{\omega_{k_1}^q \omega_{k+k_1}^q} \le \frac{1}{\omega_k^q} \left[\alpha_M^{(2)} \sum_{k_1=1}^{M} \frac{1}{\omega_{k_1}^q} + \frac{\alpha_M^{(2)}}{M^{q-1}(q-1)}\right].$$

Using Lemma A.1,

$$\begin{aligned}\sum_{k_1=1}^{k-1} \frac{\alpha_{k_1}^{(2)}}{\omega_{k_1}^q \omega_{k-k_1}^q} \quad &= \quad \sum_{k_1=1}^{M-1} \frac{\alpha_{k_1}^{(2)}}{\omega_{k_1}^q \omega_{k-k_1}^q} + \frac{1}{\omega_k^q} \sum_{k_1=M}^{k-1} \frac{\omega_k^q \alpha_{k_1}^{(2)}}{\omega_{k_1}^q \omega_{k-k_1}^q} \\ &\le \quad \frac{1}{\omega_k^q} \sum_{k_1=1}^{M-1} \frac{\alpha_{k_1}^{(2)}}{\omega_{k_1}^q \left(1-\frac{k_1}{k}\right)^q} + \frac{\alpha_M^{(2)}}{\omega_k^q} \sum_{k_1=M}^{k-1} \frac{\omega_k^q}{\omega_{k_1}^q \omega_{k-k_1}^q} \\ &\le \quad \frac{1}{\omega_k^q} \left[\sum_{k_1=1}^{M-1} \frac{\alpha_{k_1}^{(2)}}{\omega_{k_1}^q \left(1-\frac{k_1}{M}\right)^q} + \alpha_M^{(2)} \left(\sum_{k_1=1}^{k-1} \frac{\omega_k^q}{\omega_{k_1}^q \omega_{k-k_1}^q} - \sum_{k_1=1}^{M-1} \frac{\omega_k^q}{\omega_{k_1}^q \omega_{k-k_1}^q}\right)\right] \\ &\le \quad \frac{1}{\omega_k^q} \left[\sum_{k_1=1}^{M-1} \frac{\alpha_{k_1}^{(2)} M^q}{\omega_{k_1}^q \left(M-k_1\right)^q} + \alpha_M^{(2)} \left(\gamma_M - \sum_{k_1=1}^{M-1} \frac{1}{\omega_{k_1}^q}\right)\right] = \frac{1}{\omega_k^q} \Sigma_a^*.\end{aligned}$$

Hence,

$$\sum_{k_1=1}^{k-1} \frac{\alpha_{k_1}^{(2)}}{\omega_{k_1}^q \omega_{k-k_1}^q} \leq \frac{\tilde{\alpha}_M^{(2)}}{\omega_k^q} \gamma_M = \frac{1}{\omega_k^q} \Sigma_b^*.$$

Recalling that $\Sigma^* = \min\{\Sigma_a^*, \Sigma_b^*\}$, one gets that $\sum_{k_1=1}^{k-1} \frac{\alpha_{k_1}^{(2)}}{\omega_{k_1}^q \omega_{k-k_1}^q} \leq \frac{1}{\omega_k^q} \Sigma^*$. Also,

$$\sum_{k_1=1}^{\infty} \frac{\alpha_{k_1}^{(2)}}{\omega_{k_1}^q \omega_{k+k_1}^q} \leq \frac{1}{\omega_k^q} \left[\sum_{k_1=1}^{M} \frac{\alpha_{k_1}^{(2)}}{\omega_{k_1}^q} + \frac{\alpha_M^{(2)}}{M^{q-1}(q-1)} \right].$$

Combining the above inequalities, we get, for the case $k \geq M$,

$$\sum_{\substack{k_1+k_2+k_3=k \\ k_j \in \mathbb{Z}}} \frac{1}{\omega_{k_1}^q \omega_{k_2}^q \omega_{k_3}^q} \leq \frac{1}{\omega_k^q} \left[\alpha_M^{(2)} \sum_{k_1=1}^{M} \frac{1}{\omega_{k_1}^q} + \frac{2\alpha_M^{(2)}}{M^{q-1}(q-1)} + \Sigma^* \right.$$
$$\left. + \sum_{k_1=1}^{M} \frac{\alpha_{k_1}^{(2)}}{\omega_{k_1}^q} + \alpha_M^{(2)} + \alpha_0^{(2)} \right] = \frac{\alpha_k^{(3)}}{\omega_k^q}. \quad \square$$

Lemma A.5. *For any $k \in \mathbb{Z}$ with $|k| \geq M \geq 6$, we have that $\alpha_k^{(3)} \leq \alpha_M^{(3)}$.*

Proof. For $k \geq 6$, the fact that $\frac{\ln(k-1)}{k+1} \leq \frac{\ln(k-2)}{k}$ implies that $\gamma_{k+1}(q) \leq \gamma_k(q)$. By definition of $\alpha_k^{(3)}$, for $|k| \geq M$, one gets that $\alpha_k^{(3)} \leq \alpha_M^{(3)}$. $\square$

Lemma A.6. *Given $q \geq 2$ and $6 \leq \bar{M} \leq M$, define for $0 \leq k \leq \bar{M} - 1$*

$$\varepsilon_k^{(3)} = \varepsilon_k^{(3)}(q, \bar{M}, M) := \sum_{k_1=\bar{M}}^{M-k} \frac{\alpha_{k+k_1}^{(2)}}{\omega_{k_1}^q \omega_{k+k_1}^q} \tag{50}$$
$$+ \sum_{k_1=\bar{M}}^{M+k} \frac{\alpha_{k_1-k}^{(2)}}{\omega_{k_1}^q \omega_{k_1-k}^q} + \frac{\alpha_M^{(2)}}{(M+1)^q (q-1)} \left[\frac{1}{(M-k)^{q-1}} + \frac{1}{(M+k)^{q-1}} \right]$$

and for $k < 0$

$$\varepsilon_k^{(3)}(q, \bar{M}, M) := \varepsilon_{|k|}^{(3)}(q, \bar{M}, M).$$

Fix $0 \leq |k| \leq \bar{M} - 1$ and $\ell \in \{1, 2, 3\}$. Then, we have that

$$\sum_{\substack{k_1+k_2+k_3=k \\ \max\{|k_1|,\ldots,|k_\ell|\} \geq \bar{M}}} \frac{1}{\omega_{k_1}^q \omega_{k_2}^q \omega_{k_3}^q} \leq \ell \varepsilon_k^{(3)}.$$

Proof. We have that

$$\sum_{\substack{k_1+k_2+k_3=k \\ \max\{|k_1|,\ldots,|k_\ell|\} \geq \bar{M}}} \frac{1}{\omega_{k_1}^q \omega_{k_2}^q \omega_{k_3}^q} \leq \ell \sum_{\substack{k_1+k_2+k_3=k \\ |k_1| \geq M}} \frac{1}{\omega_{k_1}^q \omega_{k_2}^q \omega_{k_3}^q},$$

and

$$\sum_{\substack{k_1+k_2+k_3=k\\ |k_1|\geq \bar{M}}} \frac{1}{\omega_{k_1}^q \omega_{k_2}^q \omega_{k_3}^q} = \sum_{k_1=-\infty}^{-\bar{M}} \frac{1}{\omega_{k_1}^q} \sum_{k_2+k_3=k-k_1} \frac{1}{\omega_{k_2}^q \omega_{k_2}^q \omega_{k_3}^q} + \sum_{k_1=\bar{M}}^{\infty} \frac{1}{\omega_{k_1}^q} \sum_{k_2+k_3=k-k_1} \frac{1}{\omega_{k_2}^q \omega_{k_2}^q \omega_{k_3}^q}$$

$$\leq \sum_{k_1=\bar{M}}^{\infty} \left[\frac{\alpha_{k+k_1}^{(2)}}{\omega_{k_1}^q \omega_{k+k_1}^q} + \frac{\alpha_{k_1-k}^{(2)}}{\omega_{k_1}^q \omega_{k_1-k}^q} \right]$$

$$\leq \sum_{k_1=\bar{M}}^{M-k} \frac{\alpha_{k+k_1}^{(2)}}{\omega_{k_1}^q \omega_{k+k_1}^q} + \alpha_M^{(2)} \sum_{k_1=M-k+1}^{\infty} \frac{1}{\omega_{k_1}^q \omega_{k+k_1}^q} + \sum_{k_1=\bar{M}}^{M+k} \frac{\alpha_{k_1-k}^{(2)}}{\omega_{k_1}^q \omega_{k_1-k}^q} + \alpha_M^{(2)} \sum_{k_1=M+k+1}^{\infty} \frac{1}{\omega_{k_1}^q \omega_{k_1-k}^q}$$

$$\leq \sum_{k_1=\bar{M}}^{M-k} \frac{\alpha_{k+k_1}^{(2)}}{\omega_{k_1}^q \omega_{k+k_1}^q} + \sum_{k_1=\bar{M}}^{M+k} \frac{\alpha_{k_1-k}^{(2)}}{\omega_{k_1}^q \omega_{k_1-k}^q} + \frac{\alpha_M^{(2)}}{(M+1)^q(q-1)} \left[\frac{1}{(M-k)^{q-1}} + \frac{1}{(M+k)^{q-1}} \right] = \varepsilon_k^{(3)}. \quad \square$$

B Coefficients used to define the bounds $\boldsymbol{Y}$ and $\boldsymbol{Z}$

$k \in \{0, \dots, 3m-3\}$.	
$y_k^{(2,0)}$	$\frac{\pi^2 k^2}{\lambda_0^2}(\bar{\lambda}_1 - \bar{\lambda}_0)(\bar{a}_1 - \bar{a}_0)_k - \frac{\pi^2 k^2}{\xi^3}(\bar{\lambda}_1 - \bar{\lambda}_0)^2(\bar{a}_0)_k - 3\left(\bar{a}_0 * (\bar{a}_1 - \bar{a}_0)^2\right)_k$
$y_k^{(1,1)}$	$\frac{\pi^2 k^2}{\lambda_0^2}(\bar{\lambda}_2 - \bar{\lambda}_0)(\bar{a}_1 - \bar{a}_0)_k + \frac{\pi^2 k^2}{\lambda_0^2}(\bar{\lambda}_1 - \bar{\lambda}_0)(\bar{a}_2 - \bar{a}_0)_k$ $-\frac{2\pi^2 k^2}{\xi^3}(\bar{\lambda}_2 - \bar{\lambda}_0)(\bar{\lambda}_1 - \bar{\lambda}_0)(\bar{a}_0)_k - 6\left(\bar{a}_0 * (\bar{a}_2 - \bar{a}_0) * (\bar{a}_1 - \bar{a}_0)\right)_k$
$y_k^{(0,2)}$	$\frac{\pi^2 k^2}{\lambda_0^2}(\bar{\lambda}_2 - \bar{\lambda}_0)(\bar{a}_2 - \bar{a}_0)_k - \frac{\pi^2 k^2}{\xi^3}(\bar{\lambda}_2 - \bar{\lambda}_0)^2(\bar{a}_0)_k - 3\left(\bar{a}_0 * (\bar{a}_2 - \bar{a}_0)^2\right)_k$
$y_k^{(3,0)}$	$-\frac{\pi^2 k^2}{\xi^3}(\bar{\lambda}_1 - \bar{\lambda}_0)^2(\bar{a}_1 - \bar{a}_0)_k - \left((\bar{a}_1 - \bar{a}_0)^3\right)_k$
$y_k^{(2,1)}$	$-\frac{2\pi^2 k^2}{\xi^3}(\bar{\lambda}_2 - \bar{\lambda}_0)(\bar{\lambda}_1 - \bar{\lambda}_0)(\bar{a}_1 - \bar{a}_0)_k - \frac{\pi^2 k^2}{\xi^3}(\bar{\lambda}_1 - \bar{\lambda}_0)^2(\bar{a}_2 - \bar{a}_0)_k - 3\left((\bar{a}_2 - \bar{a}_0) * (\bar{a}_1 - \bar{a}_0)^2\right)_k$
$y_k^{(1,2)}$	$-\frac{\pi^2 k^2}{\xi^3}(\bar{\lambda}_2 - \bar{\lambda}_0)^2(\bar{a}_1 - \bar{a}_0)_k - \frac{2\pi^2 k^2}{\xi^3}(\bar{\lambda}_2 - \bar{\lambda}_0)(\bar{\lambda}_1 - \bar{\lambda}_0)(\bar{a}_2 - \bar{a}_0)_k - 3\left((\bar{a}_2 - \bar{a}_0)^2 * (\bar{a}_1 - \bar{a}_0)\right)_k$
$y_k^{(0,3)}$	$-\frac{\pi^2 k^2}{\xi^3}(\bar{\lambda}_2 - \bar{\lambda}_0)^2(\bar{a}_2 - \bar{a}_0)_k - \left((\bar{a}_2 - \bar{a}_0)^3\right)_k$

Table 3: The coefficients $y_k^{(i,j)}$.

$k \in \{-2,-1\}$.	
$z_{\mathbf{k}}^{(1,1,0)}$	$\left(\bar{\Phi}_1 - \bar{\Phi}_0\right)^T (\tilde{b}_2)_F$
$z_{\mathbf{k}}^{(1,0,1)}$	$\left(\bar{\Phi}_2 - \bar{\Phi}_0\right)^T (\tilde{b}_2)_F$
$k \in \{0,\dots,3m-3\}$.	
$z_k^{(1,0,0)}$	$\begin{cases} -3\left(\bar{a}_0^2 * \tilde{a}_I^{(2)}\right)_k, \text{ for } k < m \\ -3\left(\bar{a}_0^2 * \tilde{a}^{(2)}\right)_k, \text{ for } k \geq m \end{cases}$
$z_k^{(1,0,1)}$	$\left(\frac{\pi^2 k^2}{\lambda_0^2}(\bar{a}_2 - \bar{a}_0)_k - \frac{2\pi^2 k^2}{\lambda_0^3}(\bar{\lambda}_2 - \bar{\lambda}_0)(\bar{a}_0)_k\right)\tilde{\lambda}^{(2)} + \frac{\pi^2 k^2}{\lambda_0^2}(\bar{\lambda}_2 - \bar{\lambda}_0)(\tilde{a}^{(2)})_k - 6\left(\bar{a}_0 * (\bar{a}_2 - \bar{a}_0) * \tilde{a}^{(2)}\right)_k$
$z_k^{(1,0,2)}$	$\left(-\frac{2\pi^2 k^2}{\lambda_0^3}(\bar{\lambda}_2 - \bar{\lambda}_0)(\bar{a}_2 - \bar{a}_0)_k + \frac{3\pi^2 k^2}{\xi^4}(\bar{\lambda}_2 - \bar{\lambda}_0)^2(\bar{a}_0)_k\right)\tilde{\lambda}^{(2)} - \frac{\pi^2 k^2}{\xi^3}(\bar{\lambda}_2 - \bar{\lambda}_0)^2(\tilde{a}^{(2)})_k - 3\left((\bar{a}_2 - \bar{a}_0)^2 * \tilde{a}^{(2)}\right)_k$
$z_k^{(1,0,3)}$	$\frac{3\pi^2 k^2}{\xi^4}(\bar{\lambda}_2 - \bar{\lambda}_0)^2(\bar{a}_2 - \bar{a}_0)_k\tilde{\lambda}^{(2)}$
$z_k^{(1,1,0)}$	$\left(\frac{\pi^2 k^2}{\lambda_0^2}(\bar{a}_1 - \bar{a}_0)_k - \frac{2\pi^2 k^2}{\lambda_0^3}(\bar{\lambda}_1 - \bar{\lambda}_0)(\bar{a}_0)_k\right)\tilde{\lambda}^{(2)} + \frac{\pi^2 k^2}{\lambda_0^2}(\bar{\lambda}_1 - \bar{\lambda}_0)(\tilde{a}^{(2)})_k - 6\left(\bar{a}_0 * (\bar{a}_1 - \bar{a}_0) * \tilde{a}^{(2)}\right)_k$
$z_k^{(1,1,1)}$	$\left(-\frac{2\pi^2 k^2}{\lambda_0^3}(\bar{\lambda}_2 - \bar{\lambda}_0)(\bar{a}_1 - \bar{a}_0)_k - \frac{2\pi^2 k^2}{\lambda_0^3}(\bar{\lambda}_1 - \bar{\lambda}_0)(\bar{a}_2 - \bar{a}_0)_k + \frac{6\pi^2 k^2}{\xi^4}(\bar{\lambda}_2 - \bar{\lambda}_0)(\bar{\lambda}_1 - \bar{\lambda}_0)(\bar{a}_0)_k\right)\tilde{\lambda}^{(2)}$ $-\frac{2\pi^2 k^2}{\xi^3}(\bar{\lambda}_2 - \bar{\lambda}_0)(\bar{\lambda}_1 - \bar{\lambda}_0)(\tilde{a}^{(2)})_k - 6\left((\bar{a}_2 - \bar{a}_0) * (\bar{a}_1 - \bar{a}_0) * \tilde{a}^{(2)}\right)_k$
$z_k^{(1,1,2)}$	$\left(\frac{3\pi^2 k^2}{\xi^4}(\bar{\lambda}_2 - \bar{\lambda}_0)^2(\bar{a}_1 - \bar{a}_0)_k + \frac{6\pi^2 k^2}{\xi^4}(\bar{\lambda}_2 - \bar{\lambda}_0)(\bar{\lambda}_1 - \bar{\lambda}_0)(\bar{a}_2 - \bar{a}_0)_k\right)\tilde{\lambda}^{(2)}$
$z_k^{(1,2,0)}$	$\left(-\frac{2\pi^2 k^2}{\lambda_0^3}(\bar{\lambda}_1 - \bar{\lambda}_0)(\bar{a}_1 - \bar{a}_0)_k + \frac{3\pi^2 k^2}{\xi^4}(\bar{\lambda}_1 - \bar{\lambda}_0)^2(\bar{a}_0)_k\right)\tilde{\lambda}^{(2)} - \frac{\pi^2 k^2}{\xi^3}(\bar{\lambda}_1 - \bar{\lambda}_0)^2(\tilde{a}^{(2)})_k - 3\left((\bar{a}_1 - \bar{a}_0)^2 * \tilde{a}^{(2)}\right)_k$
$z_k^{(1,2,1)}$	$\left(\frac{6\pi^2 k^2}{\xi^4}(\bar{\lambda}_2 - \bar{\lambda}_0)(\bar{\lambda}_1 - \bar{\lambda}_0)(\bar{a}_1 - \bar{a}_0)_k + \frac{3\pi^2 k^2}{\xi^4}(\bar{\lambda}_1 - \bar{\lambda}_0)^2(\bar{a}_2 - \bar{a}_0)_k\right)\tilde{\lambda}^{(2)}$
$z_k^{(1,3,0)}$	$\frac{3\pi^2 k^2}{\xi^4}(\bar{\lambda}_1 - \bar{\lambda}_0)^2(\bar{a}_1 - \bar{a}_0)_k\tilde{\lambda}^{(2)}$
$z_k^{(2,0,0)}$	$-\frac{2\pi^2 k^2}{\lambda_0^3}(\bar{a}_0)_k\tilde{\lambda}^{(1)}\tilde{\lambda}^{(2)} - 6\left(\bar{a}_0 * \tilde{a}^{(1)} * \tilde{a}^{(2)}\right)_k$
$z_k^{(2,0,1)}$	$\left(-\frac{2\pi^2 k^2}{\lambda_0^3}(\bar{a}_2 - \bar{a}_0)_k + \frac{6\pi^2 k^2}{\xi^4}(\bar{\lambda}_2 - \bar{\lambda}_0)(\bar{a}_0)_k\right)\tilde{\lambda}^{(1)}\tilde{\lambda}^{(2)} - 6\left((\bar{a}_2 - \bar{a}_0) * \tilde{a}^{(1)} * \tilde{a}^{(2)}\right)_k$
$z_k^{(2,0,2)}$	$\frac{6\pi^2 k^2}{\xi^4}(\bar{\lambda}_2 - \bar{\lambda}_0)(\bar{a}_2 - \bar{a}_0)_k\tilde{\lambda}^{(1)}\tilde{\lambda}^{(2)}$
$z_k^{(2,1,0)}$	$\left(-\frac{2\pi^2 k^2}{\lambda_0^3}(\bar{a}_1 - \bar{a}_0)_k + \frac{6\pi^2 k^2}{\xi^4}(\bar{\lambda}_1 - \bar{\lambda}_0)(\bar{a}_0)_k\right)\tilde{\lambda}^{(1)}\tilde{\lambda}^{(2)} - 6\left((\bar{a}_1 - \bar{a}_0) * \tilde{a}^{(1)} * \tilde{a}^{(2)}\right)_k$
$z_k^{(2,1,1)}$	$\left(\frac{6\pi^2 k^2}{\xi^4}(\bar{\lambda}_2 - \bar{\lambda}_0)(\bar{a}_1 - \bar{a}_0)_k + \frac{6\pi^2 k^2}{\xi^4}(\bar{\lambda}_1 - \bar{\lambda}_0)(\bar{a}_2 - \bar{a}_0)_k\right)\tilde{\lambda}^{(1)}\tilde{\lambda}^{(2)}$
$z_k^{(2,2,0)}$	$\frac{6\pi^2 k^2}{\xi^4}(\bar{\lambda}_1 - \bar{\lambda}_0)(\bar{a}_1 - \bar{a}_0)_k\tilde{\lambda}^{(1)}\tilde{\lambda}^{(2)}$
$z_k^{(3,0,0)}$	$\frac{3\pi^2 k^2}{\xi^4}(\bar{a}_0)_k(\tilde{\lambda}^{(1)})^2\tilde{\lambda}^{(2)} - 3\left((\tilde{a}^{(1)})^2 * \tilde{a}^{(2)}\right)_k$
$z_k^{(3,0,1)}$	$\frac{3\pi^2 k^2}{\xi^4}(\bar{a}_2 - \bar{a}_0)_k(\tilde{\lambda}^{(1)})^2\tilde{\lambda}^{(2)}$
$z_k^{(3,1,0)}$	$\frac{3\pi^2 k^2}{\xi^4}(\bar{a}_1 - \bar{a}_0)_k(\tilde{\lambda}^{(1)})^2\tilde{\lambda}^{(2)}$

Table 4: The coefficients $z_k^{(\ell,i,j)}$.

$k \in \{-2,-1\}$.	
$\hat{z}^{(1)}_{\mathbf{k}}$	$\left\|(\bar{\Phi}_1-\bar{\Phi}_0)^T\right\|\omega_F^{-q}+\left\|(\bar{\Phi}_2-\bar{\Phi}_0)^T\right\|\omega_F^{-q}$
$k \geq 0$.	
$\hat{z}^{(1)}_k$	$3\hat{z}^{(0)}_k+\left\|\frac{\pi^2k^2}{\lambda_0^2}(\bar{a}_2-\bar{a}_0)_k-\frac{2\pi^2k^2}{\lambda_0^3}(\bar{\lambda}_2-\bar{\lambda}_0)(\bar{a}_0)_k\right\|+\frac{\pi^2k^2}{\lambda_0^2}\lvert\bar{\lambda}_2-\bar{\lambda}_0\rvert\omega_k^{-q}+6\left(\lvert\bar{a}_0\rvert*\lvert\bar{a}_2-\bar{a}_0\rvert*\omega^{-q}\right)_k$ $+\left\|-\frac{2\pi^2k^2}{\lambda_0^3}(\bar{\lambda}_2-\bar{\lambda}_0)(\bar{a}_2-\bar{a}_0)_k+\frac{3\pi^2k^2}{\xi^4}(\bar{\lambda}_2-\bar{\lambda}_0)^2(\bar{a}_0)_k\right\|+\frac{\pi^2k^2}{\lvert\xi^3\rvert}(\bar{\lambda}_2-\bar{\lambda}_0)^2\omega_k^{-q}+3\left(\lvert\bar{a}_2-\bar{a}_0\rvert^2*\omega^{-q}\right)_k$ $+\frac{3\pi^2k^2}{\xi^4}(\bar{\lambda}_2-\bar{\lambda}_0)^2\lvert(\bar{a}_2-\bar{a}_0)_k\rvert+\left\|\frac{\pi^2k^2}{\lambda_0^2}(\bar{a}_1-\bar{a}_0)_k-\frac{2\pi^2k^2}{\lambda_0^3}(\bar{\lambda}_1-\bar{\lambda}_0)(\bar{a}_0)_k\right\|+\frac{\pi^2k^2}{\lambda_0^2}\lvert\bar{\lambda}_1-\bar{\lambda}_0\rvert\omega_k^{-q}$ $+6\left(\lvert\bar{a}_0\rvert*\lvert\bar{a}_1-\bar{a}_0\rvert*\omega^{-q}\right)_k+\left\|-\frac{2\pi^2k^2}{\lambda_0^3}(\bar{\lambda}_2-\bar{\lambda}_0)(\bar{a}_1-\bar{a}_0)_k-\frac{2\pi^2k^2}{\lambda_0^3}(\bar{\lambda}_1-\bar{\lambda}_0)(\bar{a}_2-\bar{a}_0)_k+\frac{6\pi^2k^2}{\xi^4}(\bar{\lambda}_2-\bar{\lambda}_0)(\bar{\lambda}_1-\bar{\lambda}_0)(\bar{a}_0)_k\right\|$ $+\frac{2\pi^2k^2}{\lvert\xi^3\rvert}\lvert\bar{\lambda}_2-\bar{\lambda}_0\rvert\lvert\bar{\lambda}_1-\bar{\lambda}_0\rvert\omega_k^{-q}+6\left(\lvert\bar{a}_2-\bar{a}_0\rvert*\lvert\bar{a}_1-\bar{a}_0\rvert*\omega^{-q}\right)_k$ $+\left\|\frac{3\pi^2k^2}{\xi^4}(\bar{\lambda}_2-\bar{\lambda}_0)^2(\bar{a}_1-\bar{a}_0)_k+\frac{6\pi^2k^2}{\xi^4}(\bar{\lambda}_2-\bar{\lambda}_0)(\bar{\lambda}_1-\bar{\lambda}_0)(\bar{a}_2-\bar{a}_0)_k\right\|$ $+\left\|-\frac{2\pi^2k^2}{\lambda_0^3}(\bar{\lambda}_1-\bar{\lambda}_0)(\bar{a}_1-\bar{a}_0)_k+\frac{3\pi^2k^2}{\xi^4}(\bar{\lambda}_1-\bar{\lambda}_0)^2(\bar{a}_0)_k\right\|+\frac{\pi^2k^2}{\lvert\xi^3\rvert}(\bar{\lambda}_1-\bar{\lambda}_0)^2\omega_k^{-q}+3\left((\bar{a}_1-\bar{a}_0)^2*\omega^{-q}\right)_k$ $+\left\|\frac{6\pi^2k^2}{\xi^4}(\bar{\lambda}_2-\bar{\lambda}_0)(\bar{\lambda}_1-\bar{\lambda}_0)(\bar{a}_1-\bar{a}_0)_k+\frac{3\pi^2k^2}{\xi^4}(\bar{\lambda}_1-\bar{\lambda}_0)^2(\bar{a}_2-\bar{a}_0)_k\right\|+\frac{3\pi^2k^2}{\xi^4}(\bar{\lambda}_1-\bar{\lambda}_0)^2\lvert(\bar{a}_1-\bar{a}_0)_k\rvert$
$\hat{z}^{(2)}_k$	$\frac{2\pi^2k^2}{\lvert\lambda_0^3\rvert}\lvert(\bar{a}_0)_k\rvert+6\left(\lvert\bar{a}_0\rvert*(\omega^{-q})^2\right)_k+\left\|-\frac{2\pi^2k^2}{\lambda_0^3}(\bar{a}_2-\bar{a}_0)_k+\frac{6\pi^2k^2}{\xi^4}(\bar{\lambda}_2-\bar{\lambda}_0)(\bar{a}_0)_k\right\|+6\left(\lvert\bar{a}_2-\bar{a}_0\rvert*(\omega^{-q})^2\right)_k$ $+\frac{6\pi^2k^2}{\xi^4}\lvert\bar{\lambda}_2-\bar{\lambda}_0\rvert\lvert(\bar{a}_2-\bar{a}_0)_k\rvert+\left\|-\frac{2\pi^2k^2}{\lambda_0^3}(\bar{a}_1-\bar{a}_0)_k+\frac{6\pi^2k^2}{\xi^4}(\bar{\lambda}_1-\bar{\lambda}_0)(\bar{a}_0)_k\right\|+6\left(\lvert\bar{a}_1-\bar{a}_0\rvert*(\omega^{-q})^2\right)_k$ $+\left\|\frac{6\pi^2k^2}{\xi^4}(\bar{\lambda}_2-\bar{\lambda}_0)(\bar{a}_1-\bar{a}_0)_k+\frac{6\pi^2k^2}{\xi^4}(\bar{\lambda}_1-\bar{\lambda}_0)(\bar{a}_2-\bar{a}_0)_k\right\|+\frac{6\pi^2k^2}{\xi^4}\lvert\bar{\lambda}_1-\bar{\lambda}_0\rvert\lvert(\bar{a}_1-\bar{a}_0)_k\rvert$
$\hat{z}^{(3)}_k$	$\frac{3\pi^2k^2}{\xi^4}\lvert(\bar{a}_0)_k\rvert+3\left((\omega^{-q})^3\right)_k+\frac{3\pi^2k^2}{\xi^4}\lvert(\bar{a}_2-\bar{a}_0)_k\rvert+\frac{3\pi^2k^2}{\xi^4}\lvert(\bar{a}_1-\bar{a}_0)_k\rvert$

Table 5: The bounds $\hat{z}^{(\ell)}_k$. For $k \in \{0,\dots,m-1\}$, $\hat{z}^{(0)}_k = \left(\lvert\bar{a}_0\rvert^2*\omega_I^{-q}\right)_k$, where $(\omega_I^{-q})_k = 0$ if $\lvert k\rvert < m$ and $(\omega_I^{-q})_k = \omega_k^{-q}$ otherwise. For $k \geq m$, $\hat{z}^{(0)}_k = \left(\lvert\bar{a}_0\rvert^2*\omega^{-q}\right)_k$.

$\tilde{Z}^{(1)}_M$	$3\left(\frac{\lambda_0}{\pi^2M^2-\lambda_0}\right)\lVert\bar{a}_0\rVert_q^2\alpha_M^{(3)}+\frac{1}{\lambda_0^2}\left(\frac{\pi^2M^2\lambda_0}{\pi^2M^2-\lambda_0}\right)\lvert\bar{\lambda}_2-\bar{\lambda}_0\rvert+6\left(\frac{\lambda_0}{\pi^2M^2-\lambda_0}\right)\lVert\bar{a}_0\rVert_q\lVert\bar{a}_2-\bar{a}_0\rVert_q\alpha_M^{(3)}+\frac{1}{\lvert\xi^3\rvert}\left(\frac{\pi^2M^2\lambda_0}{\pi^2M^2-\lambda_0}\right)(\bar{\lambda}_2-\bar{\lambda}_0)^2$ $+3\left(\frac{\lambda_0}{\pi^2M^2-\lambda_0}\right)\lVert\bar{a}_2-\bar{a}_0\rVert_q^2\alpha_M^{(3)}+\frac{1}{\lambda_0^2}\left(\frac{\pi^2M^2\lambda_0}{\pi^2M^2-\lambda_0}\right)\lvert\bar{\lambda}_1-\bar{\lambda}_0\rvert+6\left(\frac{\lambda_0}{\pi^2M^2-\lambda_0}\right)\lVert\bar{a}_0\rVert_q\lVert\bar{a}_1-\bar{a}_0\rVert_q\alpha_M^{(3)}$ $+\frac{2}{\lvert\xi^3\rvert}\left(\frac{\pi^2M^2\lambda_0}{\pi^2M^2-\lambda_0}\right)\lvert\bar{\lambda}_2-\bar{\lambda}_0\rvert\lvert\bar{\lambda}_1-\bar{\lambda}_0\rvert+6\left(\frac{\lambda_0}{\pi^2M^2-\lambda_0}\right)\lVert\bar{a}_2-\bar{a}_0\rVert_q\lVert\bar{a}_1-\bar{a}_0\rVert_q\alpha_M^{(3)}+\frac{1}{\lvert\xi^3\rvert}\left(\frac{\pi^2M^2\lambda_0}{\pi^2M^2-\lambda_0}\right)(\bar{\lambda}_1-\bar{\lambda}_0)^2$ $+3\left(\frac{\lambda_0}{\pi^2M^2-\lambda_0}\right)\lVert\bar{a}_1-\bar{a}_0\rVert_q^2\alpha_M^{(3)}$
$\tilde{Z}^{(2)}_M$	$6\left(\frac{\lambda_0}{\pi^2M^2-\lambda_0}\right)\lVert\bar{a}_0\rVert_q\alpha_M^{(3)}+6\left(\frac{\lambda_0}{\pi^2M^2-\lambda_0}\right)\lVert\bar{a}_2-\bar{a}_0\rVert_q\alpha_M^{(3)}+6\left(\frac{\lambda_0}{\pi^2M^2-\lambda_0}\right)\lVert\bar{a}_1-\bar{a}_0\rVert_q\alpha_M^{(3)}$
$\tilde{Z}^{(3)}_M$	$3\left(\frac{\lambda_0}{\pi^2M^2-\lambda_0}\right)\alpha_M^{(3)}$

Table 6: The bounds $\tilde{Z}^{(\ell)}_M$, for $\ell = 1,2,3$.

References

[1] Jan Bouwe van den Berg, Jean-Philippe Lessard, and Konstantin Mischaikow. Global smooth solution curves using rigorous branch following. *Math. Comp.*, 79(271):1565–1584, 2010.

[2] Michael Plum. Existence and enclosure results for continua of solutions of parameter-dependent nonlinear boundary value problems. *J. Comput. Appl. Math.*, 60(1-2):187–200, 1995. Linear/nonlinear iterative methods and verification of solution (Matsuyama, 1993).

[3] Sarah Day, Yasuaki Hiraoka, Konstantin Mischaikow, and Toshi Ogawa. Rigorous numerics for global dynamics: a study of the Swift-Hohenberg equation. *SIAM J. Appl. Dyn. Syst.*, 4(1):1–31 (electronic), 2005.

[4] Stanislaus Maier-Paape, Ulrich Miller, Konstantin Mischaikow, and Thomas Wanner. Rigorous numerics for the Cahn-Hilliard equation on the unit square. *Rev. Mat. Complut.*, 21(2):351–426, 2008.

[5] Jean-Philippe Lessard. Recent advances about the uniqueness of the slowly oscillating periodic solutions of Wright's equation. *J. Differential Equations*, 248(5):992–1016, 2010.

[6] Michael E. Henderson. Multiple parameter continuation: computing implicitly defined k-manifolds. *Internat. J. Bifur. Chaos Appl. Sci. Engrg.*, 12(3):451–476, 2002.

[7] M. L. Brodzik and W. C. Rheinboldt. The computation of simplicial approximations of implicitly defined two-dimensional manifolds. *Comput. Math. Appl.*, 28(9):9–21, 1994.

[8] M. L. Brodzik. The computation of simplicial approximations of implicitly defined p-dimensional manifolds. *Comput. Math. Appl.*, 36(6):93–113, 1998.

[9] R. Melville and D. S. Mackey. A new algorithm for two-dimensional numerical continuation. *Comput. Math. Appl.*, 30(1):31–46, 1995.

[10] Eugene Allgower and Kurt Georg. Simplicial and continuation methods for approximating fixed points and solutions to systems of equations. *SIAM Rev.*, 22(1):28–85, 1980.

[11] Maxime Breden, Jean-Philippe Lessard, and Matthieu Vanicat. Global Bifurcation Diagrams of Steady States of Systems of PDEs via Rigorous Numerics: a 3-Component Reaction-Diffusion System. *Acta Appl. Math.*, 128:113–152, 2013.

[12] Wolf-Jürgen Beyn and Eusebius Doedel. Stability and multiplicity of solutions to discretizations of nonlinear ordinary differential equations. *SIAM J. Sci. Statist. Comput.*, 2(1):107–120, 1981.

[13] Marcio Gameiro and Jean-Philippe Lessard. Analytic estimates and rigorous continuation for equilibria of higher-dimensional PDEs. *J. Differential Equations*, 249(9):2237–2268, 2010.

[14] Shui Nee Chow and Jack K. Hale. *Methods of bifurcation theory*, volume 251 of *Grundlehren der Mathematischen Wissenschaften [Fundamental Principles of Mathematical Science]*. Springer-Verlag, New York, 1982.

[15] Marcio Gameiro and Jean-Philippe Lessard. Efficient Rigorous Numerics for Higher-Dimensional PDEs via One-Dimensional Estimates. *SIAM J. Numer. Anal.*, 51(4):2063–2087, 2013.

[16] Werner C. Rheinboldt. On the computation of multidimensional solution manifolds of parametrized equations. *Numer. Math.*, 53(1-2):165–181, 1988.

[17] L. Dieci and T. Eirola. Numerical dynamical systems. Lecture Notes, 2005.

[18] Nelson Dunford and Jacob T. Schwartz. *Linear operators. Part I.* Wiley Classics Library. John Wiley & Sons Inc., New York, 1988. General theory, With the assistance of William G. Bade and Robert G. Bartle, Reprint of the 1958 original, A Wiley-Interscience Publication.

[19] J. W. Cahn and J. E. Hilliard. Free energy of a nonuniform system i. interfacial free energy. *Journal of Chemical Physics*, 28:258–267, 1958.

[20] Marcio Gameiro, Jean-Philippe Lessard, and Konstantin Mischaikow. Validated continuation over large parameter ranges for equilibria of PDEs. *Math. Comput. Simulation*, 79(4):1368–1382, 2008.

[21] S.M. Rump. INTLAB - INTerval LABoratory. In Tibor Csendes, editor, *Developments in Reliable Computing*, pages 77–104. Kluwer Academic Publishers, Dordrecht, 1999. http://www.ti3.tu-harburg.de/rump/.

[22] Luca Dieci, Maria Grazia Gasparo, and Alessandra Papini. Path following by svd. In *Computational Science–ICCS 2006*, pages 677–684. Springer, 2006.

[23] Jan Bouwe van den Berg, Jason D. Mireles-James, Jean-Philippe Lessard, and Konstantin Mischaikow. Rigorous numerics for symmetric connecting orbits: even homoclinics of the Gray-Scott equation. *SIAM J. Math. Anal.*, 43(4):1557–1594, 2011.

[24] Marcio Gameiro, Jean-Philippe Lessard, and Alessandro Pugliese. MATLAB codes. `http://archimede.mat.ulaval.ca/jplessard/galepu`